MAGNETIC PHASE TRANSITIONS AND EXCHANGE INTERACTIONS IN $TbMnO_3$: SYMMETRY ANALYSIS

ARASH ALAM-SAMIMI

Magnetic Phase Transitions and Exchange Interactions in $TbMnO_3$: Symmetry Analysis

by

© Arash A. Samimi
BSc (2005) Tehran Azad University - Tehran - Iran

A thesis submitted to the
School of Graduate Studies
in partial fulfillment of the
requirements for the degree of
Master of Science.

Department of Physics and Physical Oceanography
Memorial University of Newfoundland

August 25, 2009

ST. JOHN'S NEWFOUNDLAND

Contents

Abstract

This thesis is a theoretical approach to study the magnetic phase transitions and exchange interactions in the spiral magnet $TbMnO_3$ by using group theory. First, we study the magnetic and ferroelectric transitions by considering the symmetry breaking associated with each transition. Second, we write the exchange interactions for the Mn magnetic ions in terms of the magnetic order parameters which are associated with various irreducible representations of the magnetic space group. Third, considering the exchange interactions and single ion anisotropy we examine the interactions on the whole lattice.

The most general form of the exchange interactions for Mn atoms in $TbMnO_3$ is formulated, including nearest neighbor and next-nearest neighbor interactions. Our phenomenological model also contains antisymmetric terms which lead to a mixing of spin-wave polarizations. It is found that for each exchange path there are six independent exchange terms, leading to a rather complicated Hamiltonian.

Finally, equations of motions for spin waves are derived. Particular attention is given to the high-temperature phase (phase I) with the sinusoidal antiferromagnetic arrangement of spins and the incommensurate wave vector Q. The symmetric case and the degeneracy in the spin-wave spectrum in this phase are also discussed. More complex magnetic interactions lead to the spiral phase lying in the bc plane. This is the low-temperature phase (phase II) which needs further theoretical analyses.

Acknowledgements

I was fortunate to get my Master's degree under the supervision of a theoretical physicist whose work is indeed a piece of art. Using symmetry analyses and group theory, Dr. Stephanie Curnoe's way of looking at problems has a unique sound and is full of beauty. I would like to thank Dr. Curnoe for giving me assistance, guidance and advice.

Special thanks should be given to Professor Martin Plumer for his helpful discussions and bright ideas. I would like to thank my teaching supervisor in Graduate Program in Teaching (GPT), Dr. Kristin Poduska who gave me a new insight into teaching & learning.

I am also greatly indebted to my past professor Dr. G . R. Jafari in Iran for his encouragement to pursue my graduate studies.

Last, but not least, I thank my family: my parents, Maryam and Javad, and my brother, Farshad, for their unconditional support.

List of Tables

List of Figures

Chapter 1

An Introduction to Multiferroics

1.1 Introduction

The idea of the coupling between the electric and magnetic properties in insulators goes back to 1894 when Pierre Curie postulated the magnetoelectric effect [1]. In 1959 Landau and Lifshitz gave a more sophisticated description of the linear coupling between magnetic and electric fields [2]. Following this idea the first theoretical prediction of the phenomenon was proposed by Dzyaloshinskii [3] and in 1960 Astrov observed the magnetoelectric effect in antiferromagnetics [4]. Another challenging idea was the coexistence of the spontaneous electric polarization (ferroelectricity) and spontaneous magnetization in a single material in the absence of an external magnetic or electric field. This kind of materials was later known as multiferroics [5].

Several multiferroics have been discovered up to now including some boracites, fluorides, hexagonal manganites and perovskites. Multiferroics are the materials with simultaneous ferroic properties. Ferroelectricity, (anti)ferromagnetism and ferroelasticity exist together in one material and can be controlled by each other. In this thesis we are considering the magnetoelectric interactions and predominantly the coexistence of magnetization and

ferroelectricity.

Multiferroics can be classified into two categories; type I (old class) and type II (new class). In type I multiferroics with a rather weak magnetoelectric coupling, the Curie and Neel temperatures are very different from each other and well above the room temperature. Ferroelectricity and magnetism have different origins of orders and the spontaneous polarization is rather large (10-100 $\mu C/cm^2$) [6]. A typical example is $BiFeO_3$ (BFO) with $T_C \approx 1100$ K and $T_N \approx 643$ K [7].

The field of multiferroics attracted much attention after the discovery of the large magnetoelectric effect in $TbMnO_3$ with $T_N \approx 41$ K and $T_C \approx 28$ K by Kimura *et al.* in 2003 [8, 9]. In the next chapters we will study this material in detail. In type II multiferroics with a strong magnetoelectric coupling, the Curie and Neel temperatures are pretty close to each other and ferroelectricity appears as a result of a specific spin arrangement. The noncollinear spiral spin structure, arising from competing magnetic interactions, breaks inversion symmetry and leads to polarization in a direction which is allowed by the symmetry of the material. There are different types of spiral magnetic structures including screw (spin rotation axis is parallel to the propagation vector), cycloidal (spin rotation axis is perpendicular to the propagation vector of the spiral) and conical (a ferromagnetic component coexists with a screw or cycloidal component) [10, 21]. The direction of the polarization in these materials can be controlled by applying an external magnetic field. A microscopic mechanism based on the spin supercurrent was proposed by Katsura *et al.* in 2005 which shows that ferroelectricity is induced by an inverse Dzyloshinskii-Moriya interaction in noncollinear magnets [11].

Besides the rich physics, multiferroics have several promising device applications such as electric field-tunable elements, magnetic field sensors and storage devices. Multiferroics are frustrated magnetic systems in which the competing spin interactions lower the ordering temperature [12]. Another interesting field is the search for high-temperature magnetoelectric multiferroics.

	M	P	ϵ
$\mathcal{K}$	-1	$+1$	$+1$
I	$+1$	-1	$+1$

Table 1.1: Three primary ferroic properties (polarization P, magnetization M and strain ϵ) and their sign changes under time reversal $\mathcal{K}$ and spatial inversion I.

Chapter 1 is a brief introduction to multiferroics and their microscopic mechanism. In Chapter 2, we introduce the mathematical formalism we need in order to study the phenomenology of multiferroics. The overview of the material is given in Chapter 3 which contains information about the crystal and magnetic structure of $TbMnO_3$. Finally, Chapter 4 consists of our theoretical results and discussions on the magnetic phase transitions, exchange interactions and spin-wave equations for $TbMnO_3$.

1.2 Ferroic Materials

In a ferroic material, spontaneous polarization P, magnetization M or strain ϵ lead to ferroelectricity, ferromagnetism or ferroelasticity respectively. From a symmetry point of view, the three primary ferroic properties can be characterized by their behavior under time-reversal $\mathcal{K}$ and spatial-inversion I as shown in Table 1.1. Another ferroic order parameter is ferrotoroidicity which is odd under both $\mathcal{K}$ and I. It can correspond to the coexistence of polarization and magnetization [6]. The spontaneous and stable order parameter in ferrotoroidic materials is taken to be the curl of magnetization or polarization [24].

As mentioned in Section 1.1, in type I multiferroics, (anti)ferromagnetism and ferroelectricity arise independently and the magnetoelectric coupling is weak. In type II multiferroics, the order parameters are strongly coupled and ferroelectricity is spin driven. Competing magnetic interactions give rise to a spiral magnetic order which leads to ferroelectricity. Thus,

frustrated systems are promising candidates for type II multiferroics.

1.3 Microscopic Mechanism

Katsura *et al.* proposed a microscopic mechanism of the spiral-spin-driven ferroelectricity which is based on the spin supercurrent j_s [11] and well explains the ferroelectricity of $RMnO_3$ (R = Tb and Dy) [21]. j_s is even under time reversal since the spin polarization is also reversed together with the direction. Therefore, from the symmetry point of view, j_s and P belong to the same class and a coupling between them is expected. In this model, a local polarization appears as a result of the spin current induced between noncollinearly-coupled spins at an angle ($\neq 0, \pi$). The polarization is given by [21]:

$$\mathbf{P} = \gamma[\mathbf{S}(\mathbf{r_i}) \times \mathbf{S}(\mathbf{r_{i+1}})] \times (\mathbf{r_i} - \mathbf{r_{i+1}}) \tag{1.1}$$

where γ is a constant related to the spin-orbit coupling and superexchange interactions and $r_i - r_{i+1}$ is the vector connecting two neighboring sites. This model is considered as the inverse Dzyaloshinskii-Moriya (DM) interaction where the oxygen between two coupled spins can be displaced through the spin-lattice interaction. Fig. 1.1 shows the coupled Mn ions and the oxygens between them in $TbMnO_3$. To develop a magnetic Hamiltonian we need both the symmetric ($S_i \cdot S_j$) and antisymmetric ($S_i \times S_j$) exchange interactions [13]. P. W. Anderson [14] introduced a microscopic mechanism for insulators which leads to isotropic superexchange interactions ($S_1 \cdot S_2$). The idea was based on the Coulomb repulsion and Pauli's principle. T. Moriya [15, 16, 17] extended Anderson's theory to include the antisymmetric spin coupling:

$$H = J\mathbf{S_1} \cdot \mathbf{S_2} + \mathbf{D_{12}} \cdot (\mathbf{S_1} \times \mathbf{S_2}) + \mathbf{S_1} \cdot \mathbf{\Gamma} \cdot \mathbf{S_2} + \ldots \tag{1.2}$$

where the second term is the antisymmetric Dzyaloshinsky-Moriya (DM) exchange interaction and Γ is a symmetrical tensor. The constant vector $\mathbf{D}$ is restricted to those which are

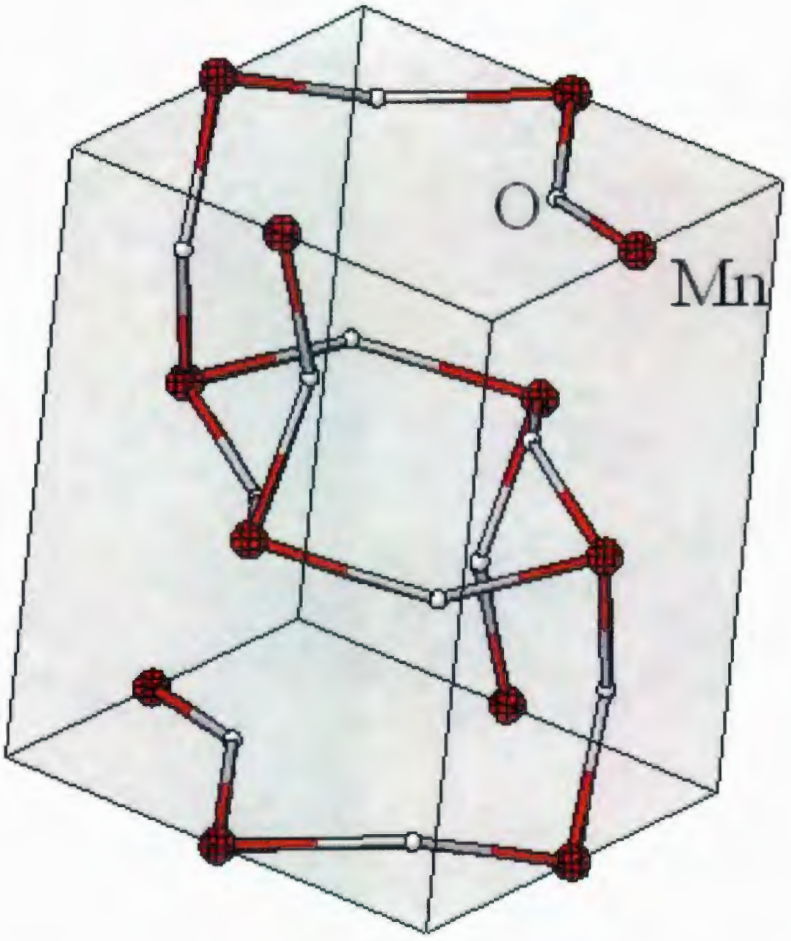

Figure 1.1: Superexchange paths with coupled Mn ions in red and the intervening O ions in white.

invariant under all symmetry operations of the space group (Moriya's rules) [15]. Sergienko *et al.* [18] argued that the coexistence and strong coupling between ferroelectricity (FE) and magnetism in perovskite manganites are due to the DM interaction. Their nearest-neighbor model is a result of the competition between the double exchange, superexchange and DM interactions. Some other theoretical arguments [12] and group theoretical approaches [19, 20] have been proposed to describe the microscopic mechanism in multiferroics.

1.4 Polarization Flop and Magnetic Memory Effect

It has been revealed that applying an external magnetic field in the multiferroic phase can change the direction and magnitude of the electric polarization in magneto-electric multiferroics [8, 25, 26, 27, 28]. In $TbMnO_3$, as a typical example, the electric polarization is completely suppressed with applying the critical magnetic field ($H_c = 7$ T) along c and the incommensurate ordering of Mn moments is destroyed. Ferroelectricity also disappears and the paraelectric phase has a commensurate antiferromagnetic ordering [28]. This is an incommensurate to commensurate transition. In the incommensurate state the proportion of spin periodicity and lattice periodicity is a fraction while in the commensurate state it is an integer.

A different behavior is observed for the magnetic field $H_c = 10.5$ T applied parallel along the a axis or $H_c = 6$ T parallel along the b axis and the polarization flops from c to a. This 90° rotation suggests a flop of the cycloidal spin plane from ab to bc. Figure 1.2 from reference [23] shows the magnetoelectric phase diagram of $TbMnO_3$ with magnetic fields along a, b and c axes. The data was obtained by measurements of dielectric constant (circles), pyroelectric or magnetoelectric current (triangles) and magnetization (diamonds). Gray regions represent the ferroelectric phases. Details on the magnetic structure at different temperature intervals will be reviewed in Chapter 3.

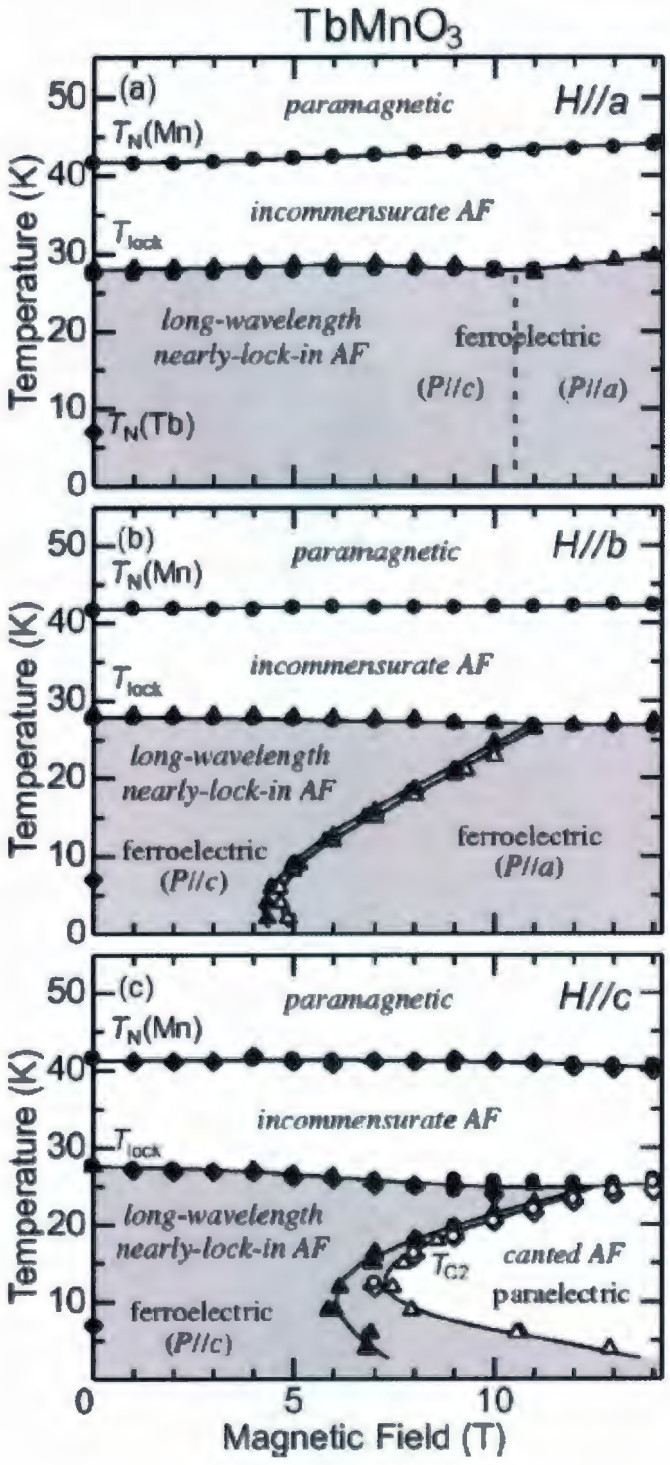

Figure 1.2: Magnetoelectric phase diagram of $TbMnO_3$ with magnetic fields along the a, b and c axes. Gray regions represent the ferroelectric phases. (From reference [23])

One of the generic features of spiral magnets such as $TbMnO_3$ at the incommensurate to commensurate transition is the magnetic memory effect. Detailed neutron scattering measurements of the propagation vector as a function of the magnetic field show that the incommensurability value for the magnetic phase obtained by cooling the system at zero field is different from the phase obtained by sweeping the field at low temperature [29]. One explanation is that a sufficiently high magnetic field induces additional domain walls which partially remain after switching off the field.

In summary, we reviewed the basic ferroic properties and their transformation under time reversal and spatial inversion. The ideas of the magnetoelectric coupling and spin-driven ferroelectricity were briefly discussed. We also argued about microscopic models and the importance of antisymmetric exchange interactions in developing a magnetic Hamiltonian. Finally, polarization flop and magnetic memory effect were discussed as the generic features of spiral magnets. With the general overview on multiferroics, we now start looking at the mathematical tools to study the behavior of our desired system $TbMnO_3$.

Chapter 2

Mathematical Tools

2.1 Group Theory and Symmetry Analysis

Symmetry analysis gives significant conclusions about our physical system and allows us to describe the phenomenology of the system in the most general way. To study the symmetry properties of the materials we use a mathematical formalism which is known as group theory. This chapter is an overview of the symmetry operators, magnetic groups and representation theory. We also discuss the symmetry of the magnetoelectric coupling term.

2.1.1 Groups

A group is a set of elements A, B, C,... with an operation called multiplication which combines any two elements to form a third one. A group has the following properties: (a) closure: the multiplication of any two elements is in the set, (b) associativity: if A,B and C are in the group then A(BC) = (AB)C, (c) identity: there is an identity element E such that EA = AE = A, (d) inverse: for each element there is an inverse such that $AA^{-1} = A^{-1}A = E$.

2.1.2 Symmetry Operators

The group elements can be considered as concrete physical symmetry operations under which the system is invariant. Consequently it is important to identify all symmetry operations to study the physical system.

The complete set of all symmetry operations of a crystal form the space group of the system. These include translations, rotations and their combinations. Setting all the translations to zero gives the point group. The fundamental operations with their standard Schoenflies notations are:

1– Rotations about axis (C_n: rotation through $2\pi/n$)

2– Reflection in planes (σ)

3– Inversion through a point (I)

Screw rotations and glide reflections are compound symmetry operations which are combinations of a rotation or reflection with a nonprimitive translation. A space group which does not involve nonprimitive translations is a symmorphic space group and if nonprimitive translations are involved to specify the space group, it is called nonsymmorphic.

We also introduce a time-reversal operation $\mathcal{K}$, which takes $t \rightarrow -t$. It basically means letting the system run back through its past history [30]. The idea of time-reversal symmetry will be important when we study the magnetic phase transitions and the different spin arrangements.

2.1.3 Crystallographic and Magnetic Groups

Real Affine Group

All translations and orthogonal transformations (rotations or rotations followed by inversion) of space form the real affine group. The elements of the group map $\mathbf{r}$ on [33]:

$$\mathbf{r}' = \alpha\mathbf{r} + \mathbf{a} \tag{2.1}$$

in a simple notation:

$$\mathbf{r}' = \{\alpha|\mathbf{a}\}\mathbf{r} \tag{2.2}$$

Thus the notation has two parts, the rotation part (orthogonal transformations) α and the translation part $\mathbf{a}$.

Space Group

The space group of a crystal contains translations and all transformations of space under which the crystal is invariant. It is in fact a subgroup of the real affine group. There are 230 space groups.

Point Group

Point groups consist of non-translational symmetry operations (rotations, reflections and inversion) that form a group. There are 32 crystallographic point groups.

Magnetic Point Group

To study the symmetry properties of magnetic crystals, we need a more general framework which contains time reversal in the crystallographic space and point groups [30]. The Shubnikov or color groups contain the time reversal operation as a symmetry operation that

interchanges black and white colors. The Shubnikov groups can be classified into three types [30, 34]:

1– The ordinary 32 point groups in which the time reversal operation is not present. Such a group is possible, for instance, in a ferromagnetic crystal with identity (E) and inversion (I) as symmetry operations.

2– The 32 gray point groups which contain the time reversal operation itself and in combination with the usual elements. Time reversal changes the sign of magnetic moments and cannot be a symmetry operation in magnetic crystals. Thus the gray group is only possible for diamagnetic or paramagnetic systems. Operations of type II Shubnikov point groups are given by:

$$\mathbf{M} = \mathbf{G} + \mathcal{K}\mathbf{G} \tag{2.3}$$

where G is the ordinary point group and $\mathcal{K}$ is time reversal.

3 - The 58 black and white or magnetic point groups which contain time reversal operation in combination with spatial rotations or reflections. Type III operations are given by:

$$\mathbf{M} = \mathbf{G} + \mathcal{K}(\mathbf{G} - \mathbf{H}) \tag{2.4}$$

where H is a halving subgroup of G.

2.1.4 Representations and Character Table

Group elements can be represented by matrices, with matrix multiplication as the group operation. A representation that cannot be block diagonalized by any unitary transformation is an irreducible representation (IR).

It is difficult to work with the representation matrices. The matrices are not unique since there is always the possibility to change the components of the basis vectors via a unitary transformation and hence the entries in the matrices. However the trace of each

D_{2h}	E	C_2^z	C_2^y	C_2^x	I	σ_z	σ_y	σ_x
A_{1g}	1	1	1	1	1	1	1	1
B_{1g}	1	1	−1	−1	1	1	−1	−1
B_{2g}	1	−1	1	−1	1	−1	1	−1
B_{3g}	1	−1	−1	1	1	−1	−1	1
A_{1u}	1	1	1	1	−1	−1	−1	−1
B_{1u}	1	1	−1	−1	−1	−1	1	1
B_{2u}	1	−1	1	−1	−1	1	−1	1
B_{3u}	1	−1	−1	1	−1	1	1	−1

Table 2.1: Character table for D_{2h}. The top row lists the group elements and the first column lists the representations.

matrix (sum of the diagonal elements) is invariant under such transformations. We define the characters $\chi(\Gamma)$ of a representation Γ of a group G as the sum over diagonal elements. The characters of each group element are listed in the character table of the group [30, 31]. As an example we look at the character table for the point group D_{2h}, shown in Table 2.1. In D_{2h} point group there are eight symmetry operations: E, C_2^z, C_2^y, C_2^x, I, σ_z, σ_y and σ_x and eight representations. Since all the representations are one dimensional, the characters indicate the effect of the symmetry operations for different representations. '1' means that the representation is invariant (symmetric) under the symmetry operation while '-1' indicates that the representation is anti-symmetric. The subscripts 'g' and 'u' in the symmetry representation labels indicate 'symmetric' or 'anti-symmetric' with respect to inversion I.

Most of the interesting properties of crystals are related to the Fourier space (k-space) of the crystal [32] and therefore it is necessary to consider the lattice in k-space. Representations of a space group are classified by the wave vector k. For each k a little group is defined as

the set of operations that leave k invariant. For example, at $k = 0$, the little group is the point group. Representations of the space group are constructed from representations of the little group for each k. For example, the k-vector $(0, k, 0)$ is invariant under the operations $\{E, C_{2y}, \sigma_x, \sigma_y\}$, so C_{2v} is the little group of $(0, k, 0)$.

2.2 Landau Theory

The Landau theory of phase transitions is a phenomenological theory which describes symmetry changes and phase transitions in the considered system [36]. Magnetization is a quantity which varies above and below the transition temperature and hence can be considered as an order parameter. In fact, order parameters are physical quantities that transform according to an IR of the space group. A magnetic order parameter such as magnetization changes sign under time reversal while polarization as the order parameter does not change sign. The Landau expansion is the expansion of a thermodynamic potential such as the free energy as a function of the order parameters and it is invariant under all symmetry elements of the space group.

2.2.1 Two Coupled Order Parameters

We are studying a multiferroic system in which magnetization and polarization are two coupled order parameters. The induced ferroelectricity depends on the magnetic order parameter and it occurs when the inversion symmetry is broken by the magnetic ordering. In the expansion for the free energy below the appearance of magnetic order induces ferroelectricity [42]:

$$f_{ME} = \alpha \chi_E^{-1} P^2 + \alpha (T - T_M) |\sigma(q)|^2 + V_{ME} \tag{2.5}$$

where P is the polarization, α is a constant, χ_E is the electric susceptibility, $\sigma(q)$ is a magnetic order parameter, V_{ME} is the magnetoelectric coupling term and T_M is the temperature at which the magnetic order appears. We define a coupling term of the form:

$$V_{ME} = \sum_{A,B=LTI,HTI} \sum_{\gamma=x,y,z} \alpha_{A,B,\gamma} \sigma_A(q)^* \sigma_B(q) P_\gamma \tag{2.6}$$

where HTI and LTI correspond to high temperature and low temperature incommensurate phases respectively. In the HTI phase the spins have a sinusoidally varying amplitude while in the LTI phase they develop a transverse order. The minimum phenomenological model is written as:

$$f = \frac{1}{2}(T - T_{HTI})|\sigma_{HTI}(q)|^2 + \frac{1}{2}(T - T_{LTI})|\sigma_{LTI}(q)|^2 + O(|\sigma(q)|^4) + \frac{1}{2}\chi_E^{-1}P^2 + V_{ME} \tag{2.7}$$

Toledano [43] developed a Landau expansion up to eighth order for $TbMnO_3$ which produces five stable states. He found the phase diagrams for these states by minimizing the free energy.

2.2.2 Symmetry of the Coupling Term

In the HTI phase σ_{LTI} is zero and V_{ME} has to be inversion invariant. For this phase no polarization can be induced. Similar symmetry argument for the HTI phase shows that the two order parameters have to be nonzero and the polarization is induced along z axis [42].

In conclusion, symmetry analysis provides us with a phenomenological model which describes the magnetic and electric phase transitions. It also shows how the symmetry properties constrain the direction of polarization. The group theoretical concepts discussed in this chapter will be used in Chapter 4 to study the magnetic phase transitions in $TbMnO_3$.

Chapter 3

Spiral Multiferroic $TbMnO_3$

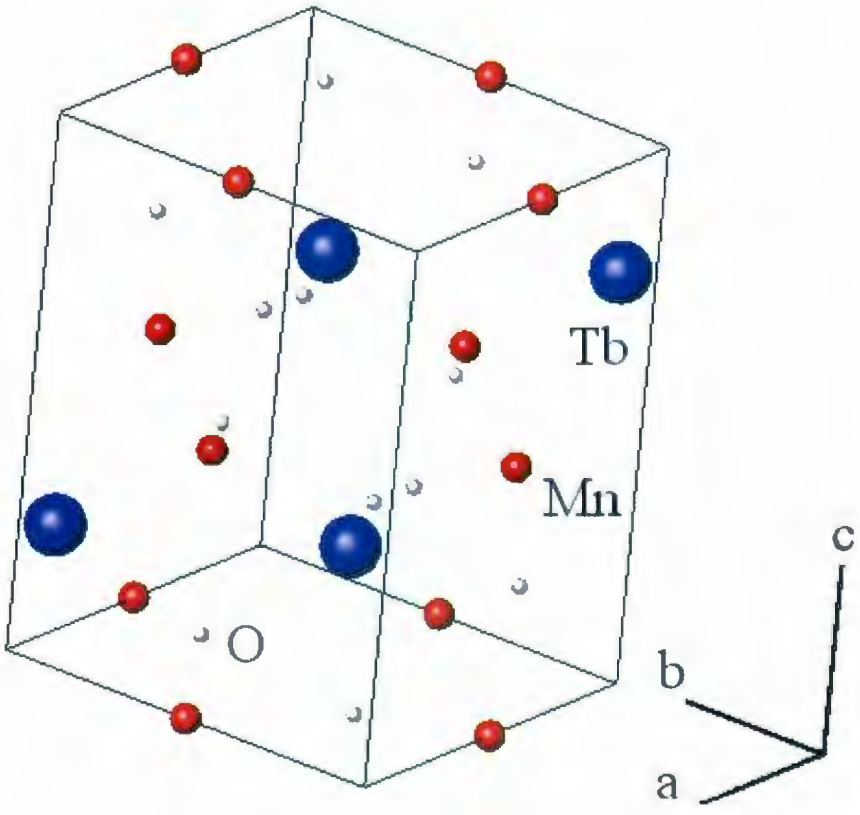

Figure 3.1: Orthorhombic unit cell of $TbMnO_3$.

This chapter presents information about the spiral multiferroic $TbMnO_3$ in two main parts: (1) crystal and magnetic structures at different temperatures and (2) a review on the experimental results related to magnetization, symmetry breaking and excitations in this material.

3.1 Crystal Structure

$TbMnO_3$ is a rare-earth manganite compound which crystallizes in an orthorhombically distorted perovskite structure [37]. The space group is *Pnma* (No. 62, D_{2h}^{16}) and the indices refer to the reflections in a, b and c planes. Most experimental papers use *Pbnm*, which is just a cyclic permutation of the indices. Here they refer to c, a and b planes, respectively, where $c = 7.4025$ Å is the longest lattice parameter, $a = 5.29314$ Å is the shortest and $b = 5.8384$ Å[38]. With four copies of the chemical formula per unit cell, the Mn atoms occupy $4b$ positions, the Tb atoms occupy $4c$ ($x = 0.9831$, $y = 0.0824$) positions and the O atoms occupy $4c$ ($x = 0.1038$, $y = 0.4667$) and $8d$ ($x = 0.7039$, $y = 0.3262$, $z = 0.0510$). Table 3.1 gives the symmetry operations and Tables 3.2, 3.3 and 3.4 give the Wyckoff positions for the two orientations of the space group. Using the character table for D_{2h} (Table 2.1) we can find out how the symmetry operations affect the Wyckoff positions (Table 3.5). As an example, operation (2) changes the positions of atom #1 with #2 and atom #3 with #4 at $4b$ positions. Table 3.6 shows the full space group effects of operations on $4b$ Wyckoff positions including lattice translations.

3.2 Magnetic Structure

Magnetization and specific heat exhibit three anomalies at $\approx$ 42 K, $\approx$ 28 K and $\approx$ 7 K [8, 9, 39]. The first and the second anomalies are due to the magnetic order of Mn moments

Operations	*Pnma*	*Pbnm*
(1) E	1	1
(2) C_{2x}	$2(0,0,\frac{1}{2})\ \frac{1}{4},0,z$	$2(\frac{1}{2},0,0)\ x,\frac{1}{4},0$
(3) C_{2z}	$2(0\frac{1}{2},0)\ 0,y,0$	$2(0,0,\frac{1}{2})\ 0,0,z$
(4) C_{2y}	$2(\frac{1}{2},0,0)\ x,\frac{1}{4},\frac{1}{4}$	$2(0,\frac{1}{2},0)\ \frac{1}{4},y,\frac{1}{4}$
(5) I	$\bar{1}\ 0,0,0$	$\bar{1}\ 0,0,0$
(6) σ_x	$a\ x,y,\frac{1}{4}$	$b\ \frac{1}{4},y,z$
(7) σ_z	$m\ x,\frac{1}{4},z$	$m\ x,y,\frac{1}{4}$
(8) σ_y	$n(0,\frac{1}{2},\frac{1}{2})\ \frac{1}{4},y,z$	$n(\frac{1}{2},0,\frac{1}{2})\ x,\frac{1}{4},z$

Table 3.1: Symmetry operations for the two different orientations of the space group.

$8d$ (O atoms)	*Pnma*	*Pbnm*
#1	x,y,z	x,y,z
#2	$\bar{x}+\frac{1}{2},\bar{y},z+\frac{1}{2}$	$x+\frac{1}{2},\bar{y}+\frac{1}{2},\bar{z}$
#3	$\bar{x},y+\frac{1}{2},\bar{z}$	$\bar{x},\bar{y},z+\frac{1}{2}$
#4	$x+\frac{1}{2},\bar{y}+\frac{1}{2},\bar{z}+\frac{1}{2}$	$\bar{x}+\frac{1}{2},y+\frac{1}{2},\bar{z}+\frac{1}{2}$
#5	$\bar{x},\bar{y},\bar{z}$	$\bar{x},\bar{y},\bar{z}$
#6	$x+\frac{1}{2},y,\bar{z}+\frac{1}{2}$	$\bar{x}+\frac{1}{2},y+\frac{1}{2},z$
#7	$x,\bar{y}+\frac{1}{2},z$	$x,y,\bar{z}+\frac{1}{2}$
#8	$\bar{x}+\frac{1}{2},y+\frac{1}{2},z+\frac{1}{2}$	$x+\frac{1}{2},\bar{y}+\frac{1}{2},z+\frac{1}{2}$

Table 3.2: Wyckoff positions for oxygen atoms at $8d$ positions. The left column lists eight oxygen atoms numbered from 1 to 8 at $8d$ positions, the middle column and the right column show the coordinates in *Pnma* and its alternative *Pbnm* space groups.

4c (Tb, O atoms)	*Pnma*	*Pbnm*
#1	$x, \frac{1}{4}, z$	$x, y, \frac{1}{4}$
#2	$\bar{x}+\frac{1}{2}, \frac{3}{4}, z+\frac{1}{2}$	$x+\frac{1}{2}, \bar{y}+\frac{1}{2}, \frac{3}{4}$
#3	$\bar{x}, \frac{3}{4}, \bar{z}$	$\bar{x}, \bar{y}, \frac{3}{4}$
#4	$x+\frac{1}{2}, \frac{1}{4}, \bar{z}+\frac{1}{2}$	$\bar{x}+\frac{1}{2}, y+\frac{1}{2}, \frac{1}{4}$

Table 3.3: Wyckoff positions for terbium and oxygen atoms at 4c positions. The left column lists terbium and oxygen numbered from 1 to 4 at 4c positions, the middle column and the right column show the coordinates in *Pnma* and its alternative *Pbnm* space groups.

4b (Mn atoms)	*Pnma*	*Pbnm*
#1	$(0, 0, \frac{1}{2})$	$(\frac{1}{2}, 0, 0)$
#2	$(\frac{1}{2}, 0, 0)$	$(0, \frac{1}{2}, 0)$
#3	$(0, \frac{1}{2}, \frac{1}{2})$	$(\frac{1}{2}, 0, \frac{1}{2})$
#4	$(\frac{1}{2}, \frac{1}{2}, 0)$	$(0, \frac{1}{2}, \frac{1}{2})$

Table 3.4: Wyckoff positions for manganese atoms at 4b positions. The left column lists four manganese atoms numbered from 1 to 4 at 4b positions, the middle column and the right column show the coordinates in *Pnma* and its alternative *Pbnm* space groups.

Operation	4*b* (Mn atoms)	4*c* (Tb, O atoms)	8*d* (O atoms)
(1) E	-	-	-
(2) C_{2x}	(1,2), (3,4)	(1,2), (3,4)	(1,2), (3,4), (5,6), (7,8)
(3) C_{2z}	(1,3), (2,4)	(1,3), (2,4)	(1,3), (2,4), (5,7), (6,8)
(4) C_{2y}	(1,4), (2,3)	(1,4), (2,3)	(1,4), (2,3), (5,8), (6,7)
(5) I	-	(1,3), (2,4)	(1,5), (2,6), (3,7), (4,8)
(6) σ_x	(1,2), (3,4)	(1,4), (2,3)	(1,6), (2,5), (3,8), (4,7)
(7) σ_z	(1,3), (2,4)	-	(1,7), (2,8), (3,5), (4,6)
(8) σ_y	(1,4), (2,3)	(1,2), (3,4)	(1,8), (2,7), (3,6), (4,5)

Table 3.5: Effects of the operations of D_{2h} on the Wyckoff positions. The left column lists the symmetry operations for D_{2h} and the other columns show how the atoms at different Wyckoff sites change positions in pairs under each symmetry operation.

while the third anomaly is related to the onset of Tb magnetic order. The simultaneous appearance of ferroelectricity and the anomaly in specific heat at ≈ 28 K suggests a coupling between the magnetic order parameter and the electric polarization. The magnetic structure of $TbMnO_3$ has been studied in four temperature intervals [9, 37, 40, 44, 39, 41] as follows:

Room Temperature

At room temperature terbium manganate is paraelectric and paramagnetic with structural properties discussed in section 3.1. Each of the Mn ions is surrounded by six oxygens in an octahedron [44].

Phase I (28 K < T < 41 K)

One of the earliest studies on the magnetic structure discovered the magnetic ordering at the $(0, k_{\mathrm{Mn}}, 0)$ wave vector. By magnetic and neutron diffraction experiments, Quezel *et al.*

OP	#1 $(h+1/2, i, j)$	#2 $(h, i+1/2, j)$	#3 $(h+1/2, i, j+1/2)$	#4 $(h, i+1/2, j+1/2)$
(1)	#1	#2	#3	#4
(2)	#2 $(-1, 2i, 2j)$	#1 $(0, 2i, 2j)$	#4 $(-1, 2i, 1+2j)$	#3 $(0, 2i, 2j+1)$
(3)	#3 $(2h+1, 2i, 0)$	#4 $(2h, 2i+1, 0)$	#1 $(2h+1, 2i, -1)$	#2 $(2h, 2i+1, -1)$
(4)	#4 $(2h, 0, 2j)$	#3 $(2h, -1, 2j)$	#2 $(2h, 0, 2j)$	#1 $(2h, -1, 2j)$
(5)	#1 $(2h+1, 2i, 2j)$	#2 $(2h, 2i+1, 2j)$	#3 $(2h+1, 2i, 2j+1)$	#4 $(2h, 2i+1, 2j+1)$
(6)	#2 $(2h+1, 1.0)$	#1 $(2h+1, 0, 0)$	#4 $(2h+1, 1, 0)$	#3 $(2h+1, 0, 0)$
(7)	#3 $(0, 0, 2j+1)$	#4 $(0, 0, 2j+1)$	#1 $(0, 0, 2j+1)$	#2 $(0, 0, 2j+1)$
(8)	#4 $(0, 2i+1, 1)$	#3 $(1, 2i+1, 1)$	#2 $(0, 2i+1, 0)$	#1 $(1, 2i+1, 0)$

Table 3.6: Full space group effects of the D_{2h} operations (OP) on 4b Wyckoff positions. The top row lists the positions of the manganese atoms numbered from 1 to 4. The left column lists the symmetry operations (OP) of D_{2h}: (1) E, (2) C_{2x}, (3) C_{2z}, (4) C_{2y}, (5) I, (6) σ_x, (7) σ_z and (8) σ_y. The manganese atoms change positions with each other under each operation. The new positions are listed in columns below each of the manganese atoms.

[37] investigated the extinction of some satellite peaks to determine the magnetic symmetry and the direction of the magnetic moments. They found that in phase I the magnetic moments on the Mn sublattice are along b axis. Below the Neel temperature ($T_N^{Mn} \approx 41K$) the Mn ions develop a sinusoidal antiferromagnetic (AF) arrangement with an incommensurate propagation wave vector $k_{\mathrm{Mn}} \approx 0.29$ while the magnetization does not exist in Tb sublattice and the ions are not ordered [39]. This phase is known as the high-temperature incommensurate (HTI) phase [42]. Figure 3.2 shows the direction and magnitude of Mn moments in phase I projected onto the bc plane.

Phase II (7 K < T < 28 K)

Below the Curie temperature $T_C^{Mn} \approx 28K$ the material is in the multiferroic state. The Mn moments transform into a cycloidal spiral spin structure with an incommensurate wave vector $k_{\mathrm{Mn}} \approx 0.28$ [39]. Magnetization is noncollinear with a component along c and a spontaneous polarization appears in the c direction. Ferroelectricity is the result of a first order transition of the electric-dipole moments associated with Mn displacements. There is no phase difference between Tb and Mn moments [9] above 7 K, and Tb sublattice displays a noncollinear order with the moments along the a axis and a wave vector $k_{Tb} \approx 0.28$ [44, 45, 46]. This phase in known as the low-temperature incommensurate (LTI) phase [42]. Figure 3.3 shows the direction and magnitude of Mn moments in phase II projected onto the bc plane and the induced polarization vector in the c direction.

Phase III (T < 7 K)

Below $T_N^{Tb} \approx 7$ K, Tb moments display an incommensurate antiferromagnetic ordering with the $k_{Tb} \approx 0.42$ wave vector [41, 44].

C_{2v}	E	C_{2y}	σ_z	σ_x
Γ_1	1	1	1	1
Γ_2	1	1	−1	−1
Γ_3	1	−1	1	−1
Γ_4	1	−1	−1	1

Table 3.7: Character table for C_{2v} lists the IR's of the little group of $(0, k, 0)$. (Adapted from reference [9])

3.3 Magnetization and Symmetry Breaking

Phase transitions and symmetry of the magnetic structure in $TbMnO_3$ were thoroughly investigated by Kenzelmann *et al.* in 2005 [9]. They showed that the magnetic phase transition into a noncollinear spiral magnetic order breaks the inversion symmetry and leads to ferroelectricity. According to x-ray diffraction measurements [47], the cycloidal spiral spin structure is accompanied by a magnetoelastically induced lattice modulation with wave numbers $k_l \approx 0.57$ at $T_N \approx 41$ K and $k_l \approx 0.55$ at $T_N \approx 28$ K. The symmetry of the magnetic structure was determined from magnetic Bragg peaks and representational analysis was used to find the irreducible representations (IR's) which describe the magnetic structure for different temperature intervals [9]. Table 3.7 shows the IR's of the little group of k for the incommensurate magnetic structure. The order parameter of the first magnetic phase transition is described by the irreducible representation Γ_3 of the little group of k while at the second transition another order parameter Γ_2 also appears. The incommensurate antiferromagnetic ordering of Tb moments below 7 K can also be described by Γ_3 and Γ_2.

3.4 Phonon and Magnon Excitations

Phonon and magnon excitations become hybridized due to DM interactions. Pimenov *et al.* [48] investigated the magnetic and magnetoelectric excitations in the terahertz (THz) frequencies by separating magnetoelectric excitations (electromagnons) from antiferromagnetic resonances (AFMR). They observed that the frequencies of two AFMR modes coincide with the electromagnon frequencies. This leads to the idea that both excitations belong to the same mode and the magnetoelectric excitations can be due to both magnetic and electric fields. Senff *et al.* [50] reported the inelastic neutron measurements to determine the magnon dispersion. Considering the work of Sneff *et al.*, Takahashi *et al.* [49] measured THz excitations using reflectance and transmittance data. They determined three exchange constants. The exchange constants are $J_1 = -0.85$ meV (ab plane), $J_2 = 0.68$ meV (ab plane) and $J_c = 1.28$ meV (c axis) and the single ion anisotropy $D = 0.13$ meV. J_1 is ferromagnetic (FM) while J_2 is antiferromagnetic (AFM). They observed an overlap and therefore a coupling between the magnon and phonon energy ranges.

This chapter was an overview of the spiral mutiferroic $TbMnO_3$ in which the crystal and magnetic structures in different temperature intervals were discussed. Phase II is the multiferroic state in which ferroelectricity is induced by the magnetic phase transitions of Mn ions into a spiral structure. Some x-ray and neutron studies determine the magnetization directions, symmetry breaking and excitations in the material which suggest a magnon-phonon hybridization.

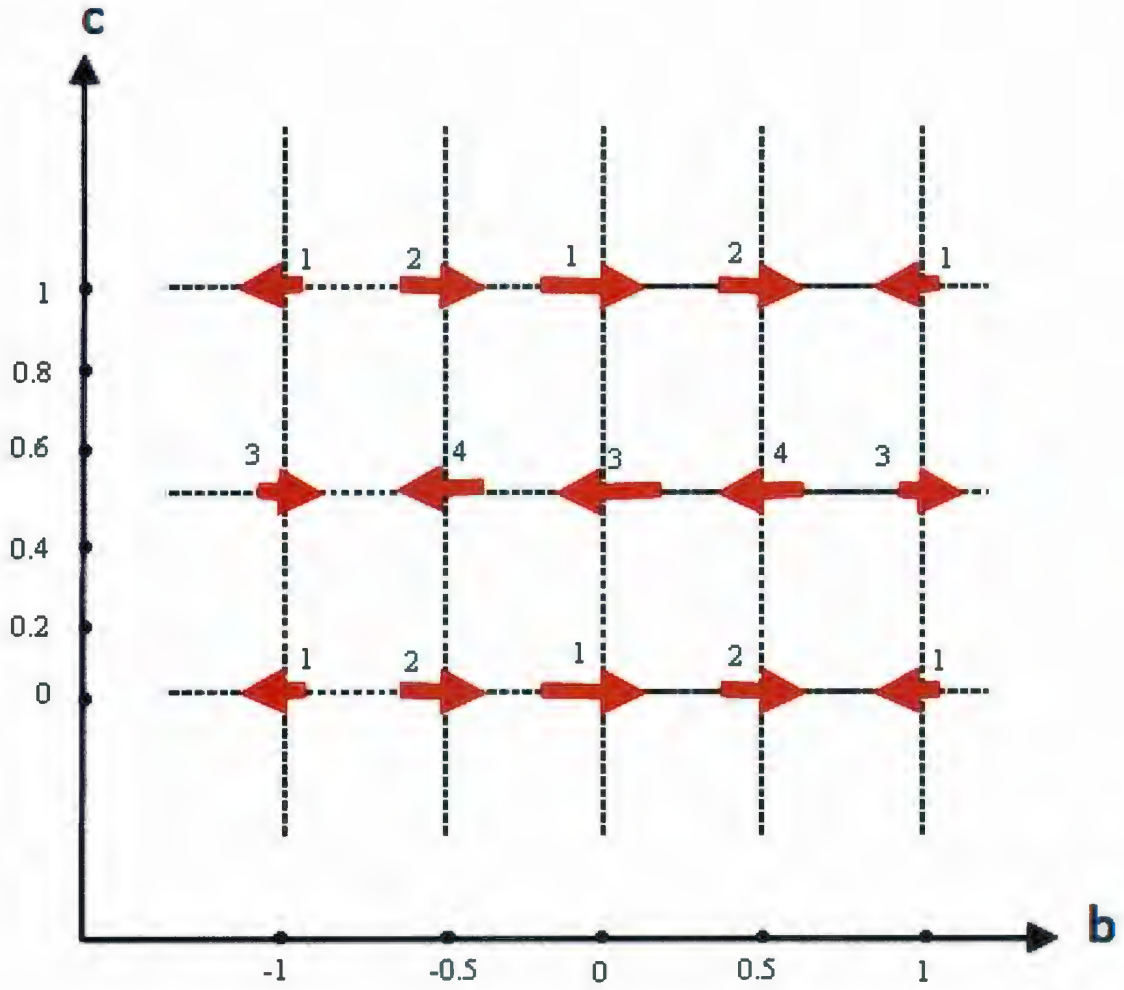

Figure 3.2: Direction and magnitude of Mn moments in phase I with the numbering of the atoms. (Adapted from reference [9])

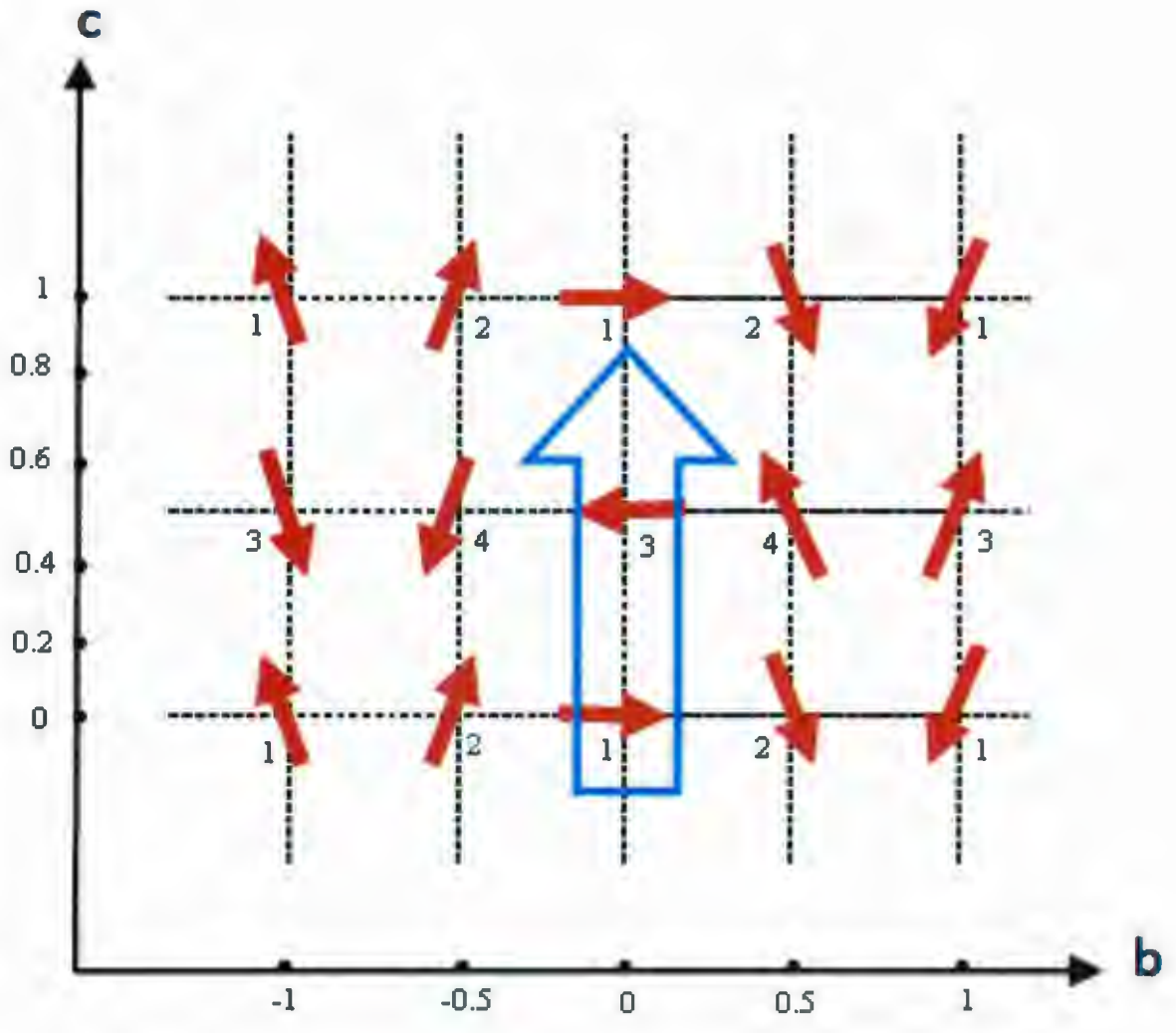

Figure 3.3: Direction and magnitude of Mn moments in phase II with the numbering of the atoms. The blue arrow shows the polarization vector. (Adapted from reference [9])

Chapter 4

Results and Discussion

This chapter contains our analytical studies of the spiral multiferroic $TbMnO_3$. Our approach includes three main parts: (1) the study of magnetic and ferroelectric phase transitions, (2) developing the most general form of the magnetic Hamiltonian and (3) the study of spin waves and their equations of motion. Connections with some experimental results are also discussed.

4.1 Magnetic Phase Transitions

To study the phase transitions we start from the symmetry elements of the parent magnetic point group in the paraelectric phase which contains the time reversal operation $\mathcal{K}$ and its combinations with the rest of the point group elements:

$$\{E, C_{2z}, C_{2y}, C_{2x}, I, \sigma_z, \sigma_y, \sigma_x, \mathcal{K}, \mathcal{K}C_{2z}, \mathcal{K}C_{2y}, \mathcal{K}C_{2x}, \mathcal{K}I, \mathcal{K}\sigma_z, \mathcal{K}\sigma_y, \mathcal{K}\sigma_x\}.$$

We begin by looking at $k = 0$ order parameters to find all the possible symmetry breaking associated with the magnetic point group. Then we extend the k-vector to $(0, k, 0)$ to find the final symmetry elements associated with each magnetic operator. Table 4.1 shows the

Magnetic IR's of D_{2h}	Applying $k=0$ Order Parameter	Extending to $(0,k,0)$
A_{1g}	$\{E, C_{2z}, C_{2y}, C_{2x}, I, \sigma_z, \sigma_y, \sigma_x\}$	$\{E, C_{2y}, \sigma_z, \sigma_x\}$
B_{1g}	$\{E, C_{2z}, I, \sigma_z, \mathcal{K}C_{2y}, \mathcal{K}C_{2x}, \mathcal{K}\sigma_y, \mathcal{K}\sigma_x\}$	$\{E, \sigma_z, \mathcal{K}C_{2y}, \mathcal{K}\sigma_x\}$
B_{2g}	$\{E, C_{2y}, I, \sigma_y, \mathcal{K}C_{2z}, \mathcal{K}C_{2x}, \mathcal{K}\sigma_z, \mathcal{K}\sigma_x\}$	$\{E, C_{2y}, \mathcal{K}\sigma_z, \mathcal{K}\sigma_x\}$
B_{3g}	$\{E, C_{2x}, I, \sigma_x, \mathcal{K}C_{2z}, \mathcal{K}C_{2y}, \mathcal{K}\sigma_z, \mathcal{K}\sigma_y\}$	$\{E, \sigma_x, \mathcal{K}C_{2y}, \mathcal{K}\sigma_z\}$
A_{1u}	$\{E, C_{2z}, C_{2y}, C_{2x}, \mathcal{K}I, \mathcal{K}\sigma_z, \mathcal{K}\sigma_y, \mathcal{K}\sigma_x\}$	$\{E, C_{2y}, \mathcal{K}\sigma_z, \mathcal{K}\sigma_x\}$
B_{1u}	$\{E, C_{2z}, \sigma_y, \sigma_x, \mathcal{K}C_{2y}, \mathcal{K}C_{2x}, \mathcal{K}I, \mathcal{K}\sigma_z\}$	$\{E, \sigma_x, \mathcal{K}C_{2y}, \mathcal{K}\sigma_z\}$
B_{2u}	$\{E, C_{2y}, \sigma_z, \sigma_x, \mathcal{K}C_{2z}, \mathcal{K}C_2x, \mathcal{K}I, \mathcal{K}\sigma_y\}$	$\{E, C_{2y}, \sigma_z, \sigma_x\}$
B_{3u}	$\{E, C_{2x}, \sigma_z, \sigma_y, \mathcal{K}C_{2z}, \mathcal{K}C_{2y}, \mathcal{K}I, \mathcal{K}\sigma_x\}$	$\{E, \sigma_z, \mathcal{K}C_{2y}, \mathcal{K}\sigma_x\}$

Table 4.1: Symmetry elements associated with each of the magnetic order parameters. The first column is a list of the representations of the point group D_{2h} (i.e. $k=0$). The second column shows the symmetry elements which remain in the presence of the point group order parameters. The third column shows the symmetry elements that remain in the presence of $(0,k,0)$.

symmetry elements that are lost by applying first a $k=0$ magnetic order parameter and then extending it to $(0,k,0)$.

Alternatively, we can begin by examining the symmetry breaking due to the k-vector, and then applying the IR's of the little group of the k. As we discussed in Section 2.1.4, for each k a little group is defined as a set of operations that leave k invariant. The little group of the k-vector $(0,k,0)$ is $C_{2v} = \{E, C_{2y}, \sigma_z, \sigma_x\}$. We use the notation from Ref. [9] which was discussed in Section 3.3 to define the representations of the little group shown in Table 3.7. After applying $(0,k,0)$ the symmetry elements are $\{E, C_{2y}, \sigma_z, \sigma_x, \mathcal{K}, \mathcal{K}C_{2y}, \mathcal{K}\sigma_z, \mathcal{K}\sigma_x\}$. Then applying the magnetic order parameters Γ_{1-4} lowers the symmetry as shown in Table 4.2 at T_N. After the first transition time reversal is broken and the spins form a sinusoidal antiferromagnetic ordering. The symmetry elements are $\{E, \mathcal{K}C_{2y}, \mathcal{K}\sigma_x, \sigma_z\}$. Thus the order

Magnetic IR's of C_{2v}	Symmetry Elements
Γ_1	$\{E, C_{2y}, \sigma_z, \sigma_x\}$
Γ_2	$\{E, C_{2y}, \mathcal{K}\sigma_z, \mathcal{K}\sigma_x\}$
Γ_3	$\{E, \sigma_z, \mathcal{K}C_{2y}, \mathcal{K}\sigma_x\}$
Γ_4	$\{E, \sigma_x, \mathcal{K}C_{2y}, \mathcal{K}\sigma_z\}$

Table 4.2: Symmetry elements associated with each magnetic order parameter of the little group of the k-vector $(0, k, 0)$.

parameter of the first transition is Γ_3.

Comparing the two approaches, we see that:

$$A_{1g}(k) \sim B_{2u}(k) = \Gamma_1 \tag{4.1}$$

$$B_{1g}(k) \sim B_{3u}(k) = \Gamma_3 \tag{4.2}$$

$$B_{2g}(k) \sim A_{1u}(k) = \Gamma_2 \tag{4.3}$$

$$B_{3g}(k) \sim B_{1u}(k) = \Gamma_4 \tag{4.4}$$

The comparison above shows that with the particular k-vector, some magnetic order parameters have the same symmetry. As we shall see, Mn moments correspond to magnetic operators that are even under inversion while Tb moments correspond to odd and even magnetic operators.

4.2 Ferroelectric Phase Transition

In the second transition into the spiral phase of spins at T_C the group loses some other elements ($\mathcal{K}C_{2y}$ and σ_z) and ferroelectricity is allowed in the c direction. Ferroelectricity in the c direction corresponds to the non-magnetic B_{1u} representations of the point group. This

$A_{1g}^{x} = +J_{1x} + J_{2x} - J_{3x} - J_{4x}$
$A_{1g}^{y} = +J_{1y} - J_{2y} - J_{3y} + J_{4y}$
$A_{1g}^{z} = +J_{1z} - J_{2z} + J_{3z} - J_{4z}$
$B_{1g}^{x} = +J_{1x} - J_{2x} - J_{3x} + J_{4x}$
$B_{1g}^{y} = +J_{1y} + J_{2y} - J_{3y} - J_{4y}$
$B_{1g}^{z} = +J_{1z} + J_{2z} + J_{3z} + J_{4z}$
$B_{2g}^{x} = +J_{1x} - J_{2x} + J_{3x} - J_{4x}$
$B_{2g}^{y} = +J_{1y} + J_{2y} + J_{3y} + J_{4y}$
$B_{2g}^{z} = +J_{1z} + J_{2z} - J_{3z} - J_{4z}$
$B_{3g}^{x} = +J_{1x} + J_{2x} + J_{3x} + J_{4x}$
$B_{3g}^{y} = +J_{1y} - J_{2y} + J_{3y} - J_{4y}$
$B_{3g}^{z} = +J_{1z} - J_{2z} - J_{3z} + J_{4z}$

Table 4.3: Magnetic operators for Mn ions at $k = 0$.

means that the symmetry elements $\{C_{2y}, C_{2x}, I, \sigma_z, \mathcal{K}C_{2y}, \mathcal{K}C_{2x}, \mathcal{K}I, \mathcal{K}\sigma_z\}$ are not allowed in the ferroelectric phase and the final symmetry elements are $\{E, \mathcal{K}\sigma_x\}$. Thus the order parameter of the second transition is Γ_2.

4.3 Magnetic Order Parameters

Tables 2.1 and 3.5 contain information about the symmetry operations and their effects on the Wyckoff positions. The information helps us to build up all the possible irreducible representations (magnetic operators) of the space group. The magnetic operators for Mn and Tb spins are shown in Table 4.3 and 4.4 respectively. We also need the inverse relations of the magnetic operators for Mn ions given in Table 4.5 to develop the exchange interactions.

Displacements have the opposite parity as the magnetic operators and are shown with

$A^x_{1u} = +J_{1x} + J_{2x} - J_{3x} - J_{4x}$
$A^y_{1u} = +J_{1y} - J_{2y} - J_{3y} + J_{4y}$
$A^z_{1g} = +J_{1z} - J_{2z} + J_{3z} - J_{4z}$
$B^x_{1u} = +J_{1x} - J_{2x} - J_{3x} + J_{4x}$
$B^y_{1u} = +J_{1y} + J_{2y} - J_{3y} - J_{4y}$
$B^z_{1g} = +J_{1z} + J_{2z} + J_{3z} + J_{4z}$
$B^x_{2g} = +J_{1x} - J_{2x} + J_{3x} - J_{4x}$
$B^y_{2g} = +J_{1y} + J_{2y} + J_{3y} + J_{4y}$
$B^z_{2u} = +J_{1z} + J_{2z} - J_{3z} - J_{4z}$
$B^x_{3g} = +J_{1x} + J_{2x} + J_{3x} + J_{4x}$
$B^y_{3g} = +J_{1y} - J_{2y} + J_{3y} - J_{4y}$
$B^z_{3u} = +J_{1z} - J_{2z} - J_{3z} + J_{4z}$

Table 4.4: Magnetic operators for Tb ions at $k = 0$.

$J_{1x} = (+A^x_{1g} + B^x_{1g} + B^x_{2g} + B^x_{3g})/4$
$J_{2x} = (+A^x_{1g} - B^x_{1g} - B^x_{2g} + B^x_{3g})/4$
$J_{3x} = (-A^x_{1g} - B^x_{1g} + B^x_{2g} + B^x_{3g})/4$
$J_{4x} = (-A^x_{1g} + B^x_{1g} - B^x_{2g} + B^x_{3g})/4$
$J_{1y} = (+A^y_{1g} + B^y_{1g} + B^y_{2g} + B^y_{3g})/4$
$J_{2y} = (-A^y_{1g} + B^y_{1g} + B^y_{2g} - B^y_{3g})/4$
$J_{3y} = (-A^y_{1g} - B^y_{1g} + B^y_{2g} + B^y_{3g})/4$
$J_{4y} = (+A^y_{1g} - B^y_{1g} + B^y_{2g} - B^y_{3g})/4$
$J_{1z} = (+A^z_{1g} + B^z_{1g} + B^z_{2g} + B^z_{3g})/4$
$J_{2z} = (-A^z_{1g} + B^z_{1g} + B^z_{2g} - B^z_{3g})/4$
$J_{3z} = (+A^z_{1g} + B^z_{1g} - B^z_{2g} - B^z_{3g})/4$
$J_{4z} = (-A^z_{1g} + B^z_{1g} - B^z_{2g} + B^z_{3g})/4$

Table 4.5: Inverse relations of the magnetic operators for Mn ions at $k = 0$.

Atoms	Displacements in terms of IR's
Mn	$3(A_{1u} \oplus B_{1u}) \oplus B_{2u} \oplus B_{3u}$
Tb	$2A_{1g} \oplus A_{1u} \oplus 2B_{1g} \oplus B_{1u} \oplus B_{2g} \oplus 2B_{2u} \oplus B_{3g} \oplus 2B_{3u}$
O	$3(A_{1g} \oplus A_{1u} \oplus B_{1g} \oplus B_{1u} \oplus B_{2g} \oplus B_{2u} \oplus B_{3g} \oplus B_{3u})$

Table 4.6: Decomposition in terms of IR's of the displacements of Mn, Tb and O atoms in $TbMnO_3$.

similar sets of representations. Table 4.6 shows the Mn, Tb and O displacements.

4.4 Exchange Interactions and Single Ion Anisotropy

Table 4.7 lists all the exchange paths less than 10 Å. There are two nearest neighbor exchange paths. Path #2 is the shortest one which is in the c direction of length $\frac{c}{2} = 3.701$ Å and pairs Mn atoms in position 1 with atoms in position 3 and atoms in position 2 with atoms in position 4. Each atom has two nearest neighbors in this path. Path #1 is the other nearest neighbor exchange path within the ab plane of length $\frac{1}{2}\sqrt{a^2+b^2} = 3.940$ Å and pairs atoms 1 with 2 and 3 with 4. For this path, each atom has four nearest neighbors. Path #8 which is similar to path #1, of length $\frac{1}{2}\sqrt{a^2+3b^2} = 9.149$ Å, connects next-nearest neighbors in the ab plane. The third path is the source of frustration that leads to the spiral magnetic phase. There are several other exchange paths that are shorter than the third path; however the third path is possibly enhanced by super exchange interactions through the $8d$ O atoms, which are only 0.63 Å away from the midpoint of the path, as shown in Fig. 1.1.

Each of the three exchange interactions is usually treated as a single, isotropic term of the form $\sum_{ij} \vec{J}_i \cdot \vec{J}_j$. Some analyses have been extended to include anti-symmetric terms of the form $\sum_{ij} \vec{D} \cdot (\vec{J}_i \times \vec{J}_j)$ where $\vec{D}$ is a constant vector. However, three symmetric and three anti-symmetric terms are allowed for a total of six independent exchange terms for each

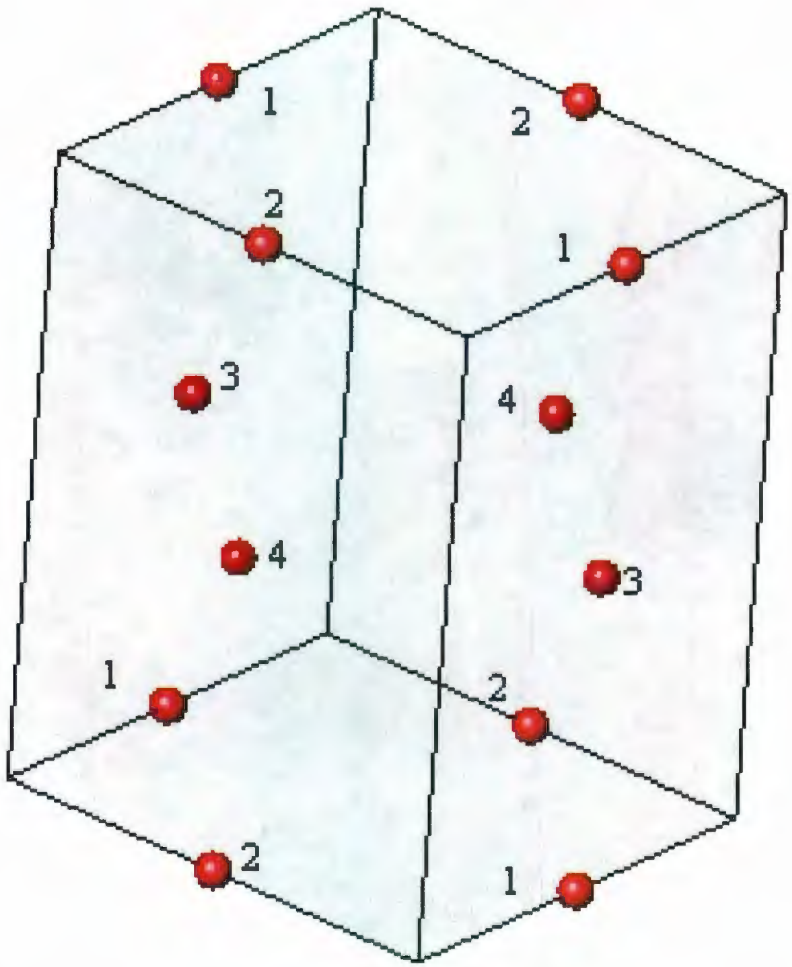

Figure 4.1: Mn sublattice with the numbering of the atoms.

path.

Spin-Spin Interactions

In the first step, we write the spin-spin interactions for paths #1, #2 and #8. The symmetry allowed exchange interactions for path #2 are shown in Table 4.8 and for paths #1 and #8 are shown in Table 4.9.

Path #	Mn n.n.	Distance	
1	(1,2), (3,4)	$\frac{1}{2}\sqrt{a^2+b^2}$	3.94031 Å
2	(1,3), (2,4)	$\frac{c}{2}$	3.70125 Å
3	(1,4), (2,3)	$\frac{1}{2}\sqrt{a^2+b^2+c^2}$	5.40604 Å
4	(1,1), (2,2) etc.	a	5.29134 Å
5	(1,1), (2,2) etc.	b	5.8384 Å
6	(1,1), (2,2) etc.	c	7.4025 Å
Path #	Mn n.n.n.		
7	(1,2), (3,4)	$\frac{1}{2}\sqrt{(3a)^2+b^2}$	8.45936 Å
8	(1,2), (3,4)	$\frac{1}{2}\sqrt{a^2+(3b)^2}$	9.14876 Å
9	(1,2), (3,4)	$\frac{1}{2}\sqrt{a^2+b^2+(2c)^2}$	8.38589 Å
10	(1,3), (2,4)	$\frac{1}{2}\sqrt{(2a)^2+c^2}$	6.45884 Å
11	(1,3), (2,4)	$\frac{1}{2}\sqrt{(2b)^2+c^2}$	6.91275 Å
12	(1,4), (2,3)	$\frac{1}{2}\sqrt{(3a)^2+b^2+c^2}$	9.23363 Å
13	(1,4), (2,3)	$\frac{1}{2}\sqrt{a^2+(3b)^2+c^2}$	9.8691 Å
14	(1,1), (2,2) etc.	$\sqrt{a^2+b^2}$	7.88062 Å
15	(1,1), (2,2) etc.	$\sqrt{a^2+c^2}$	9.1124 Å
16	(1,1), (2,2) etc.	$\sqrt{b^2+c^2}$	9.42783 Å
Path #	Mn n.n.n.n.		
17	(1,3), (2,4)	$\frac{1}{2}\sqrt{(2a)^2+(2b)^2+c^2}$	8.70652 Å

Table 4.7: Exchange paths less than 10 Å. The second column lists the atom numbers of the partners in each pair of interacting atoms.

Exchange Interactions	In Terms of the Magnetic Operators
$2J_{1x}J_{3x} + 2J_{2x}J_{4x}$	$(-A_{1g}^{x2} - B_{1g}^{x2} + B_{2g}^{x2} + B_{3g}^{x2})/4$
$J_{1x}J_{3y} - J_{2x}J_{4y} + J_{3x}J_{1y} - J_{4x}J_{2y}$	$(-A_{1g}^{x}A_{1g}^{y} - B_{1g}^{x}B_{1g}^{y} + B_{2g}^{x}B_{2g}^{y} + B_{3g}^{x}B_{3g}^{y})/4$
$J_{1x}J_{3z} - J_{2x}J_{4z} - J_{3x}J_{1z} + J_{4x}J_{2z}$	$(+A_{1g}^{x}A_{1g}^{z} + B_{1g}^{x}B_{1g}^{z} - B_{2g}^{x}B_{2g}^{z} - B_{3g}^{x}B_{3g}^{z})/4$
$2J_{1y}J_{3y} + 2J_{2y}J_{4y}$	$(-A_{1g}^{y2} - B_{1g}^{y2} + B_{2g}^{y2} + B_{3g}^{y2})/4$
$J_{1y}J_{3z} - J_{3y}J_{1z} + J_{2y}J_{4z} - J_{4y}J_{2z}$	$(+A_{1g}^{y}A_{1g}^{z} + B_{1g}^{y}B_{1g}^{z} - B_{2g}^{y}B_{2g}^{z} - B_{3g}^{y}B_{3g}^{z})/4$
$2J_{1z}J_{3z} + 2J_{2z}J_{4z}$	$(+A_{1g}^{z2} + B_{1g}^{z2} - B_{2g}^{z2} - B_{3g}^{z2})/4$

Table 4.8: Exchange interactions for path #2 (and also paths #10 and #11). The terms in each row are equal.

Exchange Interactions	In Terms of the Magnetic Operators
$2J_{1x}J_{2x} + 2J_{3x}J_{4x}$	$(+A_{1g}^{x2} - B_{1g}^{x2} - B_{2g}^{x2} + B_{3g}^{x2})/4$
$J_{1x}J_{2y} - J_{1y}J_{2x} + J_{3x}J_{4y} - J_{3y}J_{4x}$	$(-A_{1g}^{x}A_{1g}^{y} + B_{1g}^{x}B_{1g}^{y} + B_{2g}^{x}B_{2g}^{y} - B_{3g}^{x}B_{3g}^{y})/4$
$J_{1x}J_{2z} - J_{1z}J_{2x} - J_{3x}J_{4z} + J_{4x}J_{3z}$	$(-A_{1g}^{x}A_{1g}^{z} + B_{1g}^{x}B_{1g}^{z} + B_{2g}^{x}B_{2g}^{z} - B_{3g}^{x}B_{3g}^{z})/4$
$2J_{1y}J_{2y} + 2J_{3y}J_{4y}$	$(-A_{1g}^{y2} + B_{1g}^{y2} + B_{2g}^{y2} - B_{3g}^{y2})/4$
$J_{1y}J_{2z} + J_{1z}J_{2y} - J_{3y}J_{4z} - J_{3z}J_{4y}$	$(-A_{1g}^{y}A_{1g}^{z} + B_{1g}^{y}B_{1g}^{z} + B_{2g}^{y}B_{2g}^{z} - B_{3g}^{y}B_{3g}^{z})/4$
$2J_{1z}J_{2z} + 2J_{3z}J_{4z}$	$(-A_{1g}^{z2} + B_{1g}^{z2} + B_{2g}^{z2} - B_{3g}^{z2})/4$

Table 4.9: Exchange interactions for paths #1, #8 (and also #9). The terms in each row are equal.

Single Ion Anisotropy	In Terms of the Magnetic Operators
$J_{1x}^2 + J_{2x}^2 + J_{3x}^2 + J_{4x}^2$	$(A_{1g}^{x2} + B_{1g}^{x2} + B_{2g}^{x2} + B_{3g}^{x2})/4$
$J_{1x}J_{1y} - J_{2x}J_{2y} + J_{3x}J_{3y} - J_{4x}J_{4y}$	$(A_{1g}^{x}A_{1g}^{y} + B_{1g}^{x}B_{1g}^{y} + B_{2g}^{x}B_{2g}^{y} + B_{3g}^{x}B_{3g}^{y})/4$
$J_{1x}J_{1z} - J_{2x}J_{2z} - J_{3x}J_{3z} + J_{4x}J_{4z}$	$(A_{1g}^{x}A_{1g}^{z} + B_{1g}^{x}B_{1g}^{z} + B_{2g}^{x}B_{2g}^{z} + B_{3g}^{x}B_{3g}^{z})/4$
$J_{1y}^2 + J_{2y}^2 + J_{3y}^2 + J_{4y}^2$	$(A_{1g}^{y2} + B_{1g}^{y2} + B_{2g}^{y2} + B_{3g}^{y2})/4$
$J_{1z}^2 + J_{2z}^2 + J_{3z}^2 + J_{4z}^2$	$(A_{1g}^{z2} + B_{1g}^{z2} + B_{2g}^{z2} + B_{3g}^{z2})/4$
$J_{1y}J_{1z} + J_{2y}J_{2z} - J_{3y}J_{3z} - J_{4y}J_{4z}$	$(A_{1g}^{y}A_{1g}^{z} + B_{1g}^{y}B_{1g}^{z} + B_{2g}^{y}B_{2g}^{z} + B_{3g}^{y}B_{3g}^{z})/4$

Table 4.10: Single ion anisotropy terms. The terms in each row are equal.

Single Ion Anisotropy Terms

In addition, there are six single ion anisotropy terms, which include the effects of the local environment on the spin states. Table 4.10 lists all the symmetry allowed anisotropy terms.

4.5 Magnetic Hamiltonian

Now we develop the magnetic Hamiltonian including nearest neighbor and next-nearest neighbor interactions. A local magnetic operator, $\vec{J}_{j+i}$, is defined on the $\vec{i}$th atom in the $\vec{j}$th unit cell. The Fourier transform is defined over the Brillioun zone,

$$J(\vec{k}) = \sum_{i,j} \exp^{-i\vec{k}\cdot(\vec{j}+\vec{i})} J_{\vec{j}+\vec{i}} \tag{4.5}$$

where the sum over j is over all lattice sites and the sum over i is over the four local sites. We assume that the crystal contains $N_a \times N_b \times N_c$ lattice sites. We use periodic boundary conditions. The complex conjugate is

$$J(-\vec{k}) = J^*(\vec{k}). \tag{4.6}$$

$\Gamma_1^x(k) = \sum_j e^{-i\vec{k}\cdot\vec{j}}(J_{j,1}^x e^{-\vec{k}\cdot(1/2,0,0)} + J_{j,2}^x e^{-\vec{k}\cdot(0,1/2,0)} - J_{j,3}^x e^{-\vec{k}\cdot(1/2,0,1/2)} - J_{j,4}^x e^{-\vec{k}\cdot(0,1/2,1/2)})$
$\Gamma_2^x(k) = \sum_j e^{-i\vec{k}\cdot\vec{j}}(J_{j,1}^x e^{-\vec{k}\cdot(1/2,0,0)} - J_{j,2}^x e^{-\vec{k}\cdot(0,1/2,0)} + J_{j,3}^x e^{-\vec{k}\cdot(1/2,0,1/2)} - J_{j,4}^x e^{-\vec{k}\cdot(0,1/2,1/2)}$
$\Gamma_3^x(k) = \sum_j e^{-i\vec{k}\cdot\vec{j}}(J_{j,1}^x e^{-\vec{k}\cdot(1/2,0,0)} - J_{j,2}^x e^{-\vec{k}\cdot(0,1/2,0)} - J_{j,3}^x e^{-\vec{k}\cdot(1/2,0,1/2)} + J_{j,4}^x e^{-\vec{k}\cdot(0,1/2,1/2)})$
$\Gamma_4^x(k) = \sum_j e^{-i\vec{k}\cdot\vec{j}}(J_{j,1}^x e^{-\vec{k}\cdot(1/2,0,0)} + J_{j,2}^x e^{-\vec{k}\cdot(0,1/2,0)} + J_{j,3}^x e^{-\vec{k}\cdot(1/2,0,1/2)} + J_{j,4}^x e^{-\vec{k}\cdot(0,1/2,1/2)})$
$\Gamma_1^y(k) = \sum_j e^{-i\vec{k}\cdot\vec{j}}(J_{j,1}^y e^{-\vec{k}\cdot(1/2,0,0)} - J_{j,2}^y e^{-\vec{k}\cdot(0,1/2,0)} - J_{j,3}^y e^{-\vec{k}\cdot(1/2,0,1/2)} + J_{j,4}^y e^{-\vec{k}\cdot(0,1/2,1/2)})$
$\Gamma_2^y(k) = \sum_j e^{-i\vec{k}\cdot\vec{j}}(J_{j,1}^y e^{-\vec{k}\cdot(1/2,0,0)} + J_{j,2}^y e^{-\vec{k}\cdot(0,1/2,0)} + J_{j,3}^y e^{-\vec{k}\cdot(1/2,0,1/2)} + J_{j,4}^y e^{-\vec{k}\cdot(0,1/2,1/2)})$
$\Gamma_3^y(k) = \sum_j e^{-i\vec{k}\cdot\vec{j}}(J_{j,1}^y e^{-\vec{k}\cdot(1/2,0,0)} + J_{j,2}^y e^{-\vec{k}\cdot(0,1/2,0)} - J_{j,3}^y e^{-\vec{k}\cdot(1/2,0,1/2)} - J_{j,4}^y e^{-\vec{k}\cdot(0,1/2,1/2)})$
$\Gamma_4^y(k) = \sum_j e^{-i\vec{k}\cdot\vec{j}}(J_{j,1}^y e^{-\vec{k}\cdot(1/2,0,0)} - J_{j,2}^y e^{-\vec{k}\cdot(0,1/2,0)} + J_{j,3}^y e^{-\vec{k}\cdot(1/2,0,1/2)} - J_{j,4}^y e^{-\vec{k}\cdot(0,1/2,1/2)})$
$\Gamma_1^z(k) = \sum_j e^{-i\vec{k}\cdot\vec{j}}(J_{j,1}^z e^{-\vec{k}\cdot(1/2,0,0)} - J_{j,2}^z e^{-\vec{k}\cdot(0,1/2,0)} + J_{j,3}^z e^{-\vec{k}\cdot(1/2,0,1/2)} - J_{j,4}^z e^{-\vec{k}\cdot(0,1/2,1/2)})$
$\Gamma_2^z(k) = \sum_j e^{-i\vec{k}\cdot\vec{j}}(J_{j,1}^z e^{-\vec{k}\cdot(1/2,0,0)} + J_{j,2}^z e^{-\vec{k}\cdot(0,1/2,0)} - J_{j,3}^z e^{-\vec{k}\cdot(1/2,0,1/2)} - J_{j,4}^z e^{-\vec{k}\cdot(0,1/2,1/2)})$
$\Gamma_3^z(k) = \sum_j e^{-i\vec{k}\cdot\vec{j}}(J_{j,1}^z e^{-\vec{k}\cdot(1/2,0,0)} + J_{j,2}^z e^{-\vec{k}\cdot(0,1/2,0)} + J_{j,3}^z e^{-\vec{k}\cdot(1/2,0,1/2)} + J_{j,4}^z e^{-\vec{k}\cdot(0,1/2,1/2)})$
$\Gamma_4^z(k) = \sum_j e^{-i\vec{k}\cdot\vec{j}}(J_{j,1}^z e^{-\vec{k}\cdot(1/2,0,0)} - J_{j,2}^z e^{-\vec{k}\cdot(0,1/2,0)} - J_{j,3}^z e^{-\vec{k}\cdot(1/2,0,1/2)} + J_{j,4}^z e^{-\vec{k}\cdot(0,1/2,1/2)})$

Table 4.11: Magnetic operators in k-space in terms of local magnetic operators.

The inverse transform is

$$J_{\vec{j}+\vec{i}} = \frac{abc}{(2\pi)^3}\int_{\mathrm{BZ}} d^3k \exp^{i\vec{k}\cdot(\vec{j}+\vec{i})} J(\vec{k}) = \frac{abc}{(2\pi)^3}\int_{\mathrm{BZ}} d^3k \exp^{-i\vec{k}\cdot(\vec{j}+\vec{i})} J(-\vec{k}) \tag{4.7}$$

where a, b and c are the lattice constants. The orthogonality relations are:

$$\sum_{\vec{j}} e^{i(\vec{j}\cdot(\vec{k}-\vec{k}'))} = \frac{(2\pi)^3}{abc}\delta^3(k-k') \tag{4.8}$$

$$\frac{abc}{(2\pi)^3}\int_{\mathrm{BZ}} d^3k e^{i((\vec{j}-\vec{j}'+\vec{i}-\vec{i}')\cdot\vec{k})} = \delta^3_{\vec{j},\vec{j}'}\delta^3_{\vec{i},\vec{i}'} \tag{4.9}$$

Table 4.11 lists all 12 magnetic operators that transform as $\Gamma_{1,2,3,4}$ for the wave vector Q=(0,0.42,0). The inverse relations are shown in Table 4.12. As discussed earlier in this section, we look at some of the shortest exchange paths that are less than 8 Å. The shortest path is #2, which is in the z direction and couples (1,3) and (2,4). We also consider paths

$J^x_{j,1} = \frac{abc}{4(2\pi)^3}\int_{BZ} d^3k e^{i\vec{k}\cdot(\vec{j}+(1/2,0,0))}(\Gamma^x_1(k)+\Gamma^x_2(k)+\Gamma^x_3(k)+\Gamma^x_4(k))$
$J^x_{j,2} = \frac{abc}{4(2\pi)^3}\int_{BZ} d^3k e^{i\vec{k}\cdot(\vec{j}+(0,1/2,0))}(\Gamma^x_1(k)-\Gamma^x_2(k)-\Gamma^x_3(k)+\Gamma^x_4(k))$
$J^x_{j,3} = \frac{abc}{4(2\pi)^3}\int_{BZ} d^3k e^{i\vec{k}\cdot(\vec{j}+(1/2,0,1/2))}(-\Gamma^x_1(k)+\Gamma^x_2(k)-\Gamma^x_3(k)+\Gamma^x_4(k))$
$J^x_{j,4} = \frac{abc}{4(2\pi)^3}\int_{BZ} d^3k e^{i\vec{k}\cdot(\vec{j}+(0,1/2,1/2))}(-\Gamma^x_1(k)-\Gamma^x_2(k)+\Gamma^x_3(k)+\Gamma^x_4(k))$
$J^y_{j,1} = \frac{abc}{4(2\pi)^3}\int_{BZ} d^3k e^{i\vec{k}\cdot(\vec{j}+(1/2,0,0))}(\Gamma^y_1(k)+\Gamma^y_2(k)+\Gamma^y_3(k)+\Gamma^y_4(k))$
$J^y_{j,2} = \frac{abc}{4(2\pi)^3}\int_{BZ} d^3k e^{i\vec{k}\cdot(\vec{j}+(0,1/2,0))}(-\Gamma^y_1(k)+\Gamma^y_2(k)+\Gamma^y_3(k)-\Gamma^y_4(k))$
$J^y_{j,3} = \frac{abc}{4(2\pi)^3}\int_{BZ} d^3k e^{i\vec{k}\cdot(\vec{j}+(1/2,0,1/2))}(-\Gamma^y_1(k)+\Gamma^y_2(k)-\Gamma^y_3(k)+\Gamma^y_4(k))$
$J^y_{j,4} = \frac{abc}{4(2\pi)^3}\int_{BZ} d^3k e^{i\vec{k}\cdot(\vec{j}+(0,1/2,1/2))}(\Gamma^y_1(k)+\Gamma^y_2(k)-\Gamma^y_3(k)-\Gamma^y_4(k))$
$J^z_{j,1} = \frac{abc}{4(2\pi)^3}\int_{BZ} d^3k e^{i\vec{k}\cdot(\vec{j}+(1/2,0,0))}(\Gamma^z_1(k)+\Gamma^z_2(k)+\Gamma^z_3(k)+\Gamma^z_4(k))$
$J^z_{j,2} = \frac{abc}{4(2\pi)^3}\int_{BZ} d^3k e^{i\vec{k}\cdot(\vec{j}+(0,1/2,0))}(\Gamma^z_1(k)-\Gamma^z_2(k)-\Gamma^z_3(k)+\Gamma^z_4(k))$
$J^z_{j,3} = \frac{abc}{4(2\pi)^3}\int_{BZ} d^3k e^{i\vec{k}\cdot(\vec{j}+(1/2,0,1/2))}(\Gamma^z_1(k)-\Gamma^z_2(k)+\Gamma^z_3(k)-\Gamma^z_4(k))$
$J^z_{j,4} = \frac{abc}{4(2\pi)^3}\int_{BZ} d^3k e^{i\vec{k}\cdot(\vec{j}+(0,1/2,1/2))}(-\Gamma^z_1(k)-\Gamma^z_2(k)+\Gamma^z_3(k)+\Gamma^z_4(k))$

Table 4.12: Inverse relations of magnetic operators in k-space.

#1 and #8 in the ab plane which couple (1,2) and (3,4). Let the site index be (h,i,j). As an example, consider path #2 with the exchange interactions between the x components:

$$
\begin{aligned}
&2\sum_{h,i,j} J^x_{h,i,j;1}J^x_{h,i,j;3} + J^x_{h,i,j;1}J^x_{h,i,j-1;3} + J^x_{h,i,j;2}J^x_{h,i,j;4} + J^x_{h,i,j;2}J^x_{h,i,j-1;4} \\
&\quad = \frac{1}{8}\frac{abc}{(2\pi)^3}\int d^3k(e^{-ik_x/2} + e^{ik_x/2}) \\
&\quad \times[(\Gamma^x_1(k) + \Gamma^x_2(k) + \Gamma^x_3(k) + \Gamma^x_4(k))(-\Gamma^x_1(-k) + \Gamma^x_2(-k) - \Gamma^x_3(-k) + \Gamma^x_4(-k)) \\
&\quad +(\Gamma^x_1(k) - \Gamma^x_2(k) - \Gamma^x_3(k) + \Gamma^x_4(k))(-\Gamma^x_1(-k) - \Gamma^x_2(-k) + \Gamma^x_3(-k) + \Gamma^x_4(-k))] \\
&\quad = \frac{1}{2}\frac{abc}{(2\pi)^3}\int d^3k \cos\frac{k_x}{2} \\
&\quad \times[-|\Gamma^x_1(k)|^2 + |\Gamma^x_2(k)|^2 - |\Gamma^x_3(k)|^2 + |\Gamma^x_4(k)|^2 \\
&\quad +\Gamma^x_1(k)\Gamma^x_4(-k) - \Gamma^x_4(k)\Gamma^x_1(-k) - \Gamma^x_2(k)\Gamma^x_3(-k) + \Gamma^x_3(k)\Gamma^x_2(-k)]
\end{aligned}
\tag{4.10}
$$

Note that the last four terms vanish in the integral over k. As another example, for path #1 and #8, the exchange interactions between x and y components are:

$$
\begin{aligned}
&\sum_{hij} J^x_{h,i,j;1}J^y_{h,i,j;2} - J^y_{h,i,j;1}J^x_{h,i,j;2} + J^x_{h,i,j;3}J^y_{h,i,j;4} - J^y_{h,i,j;3}J^x_{h,i,j;4} \\
&\quad +J^x_{h,i,j;1}J^y_{h,i-1,j;2} - J^y_{h,i,j;1}J^x_{h,i-1,j;2} + J^x_{h,i,j;3}J^y_{h,i-1,j;4} - J^y_{h,i,j;3}J^x_{h,i-1,j;4} \\
&\quad +J^x_{h,i,j;1}J^y_{h+1,i-1,j;2} - J^y_{h,i,j;1}J^x_{h+1,i-1,j;2} + J^x_{h,i,j;3}J^y_{h+1,i-1,j;4} - J^y_{h,i,j;3}J^x_{h+1,i-1,j;4} \\
&\quad +J^x_{h,i,j;1}J^y_{h+1,i,j;2} - J^y_{h,i,j;1}J^x_{h+1,i,j;2} + J^x_{h,i,j;3}J^y_{h+1,i,j;4} - J^y_{h,i,j;3}J^x_{h+1,i,j;4} \\
&\quad = \frac{1}{16}\frac{abc}{(2\pi^3)}\int d^3k[e^{i(k_x+k_y)/2} + e^{-i(k_x+k_y)/2} + e^{i(k_x-k_y)/2} + e^{-i(k_x-k_y)/2}]
\end{aligned}
$$

$$
\begin{aligned}
&\times[(\Gamma_1^x(k)+\Gamma_2^x(k)+\Gamma_3^x(k)+\Gamma_4^x(k))(-\Gamma_1^y(-k)+\Gamma_2^y(-k)+\Gamma_3^y(-k)-\Gamma_4^y(-k)) \\
&-(\Gamma_1^y(k)+\Gamma_2^y(k)+\Gamma_3^y(k)+\Gamma_4^y(k))(\Gamma_1^x(-k)-\Gamma_2^x(-k)-\Gamma_3^x(-k)+\Gamma_4^x(-k)) \\
&+(-\Gamma_1^x(k)+\Gamma_2^x(k)-\Gamma_3^x(k)+\Gamma_4^x(k))(+\Gamma_1^y(-k)+\Gamma_2^y(-k)-\Gamma_3^y(-k)-\Gamma_4^y(-k)) \\
&-(-\Gamma_1^y(k)+\Gamma_2^y(k)-\Gamma_3^y(k)+\Gamma_4^y(k))(-\Gamma_1^x(-k)-\Gamma_2^x(-k)+\Gamma_3^x(-k)+\Gamma_4^x(-k))] \\
&=\frac{1}{4}\frac{abc}{(2\pi)^3}\int d^3k[\cos(k_x+k_y)/2+\cos(k_x-k_y)/2] \\
&\times[-\Gamma_1^x(k)\Gamma_1^y(-k)+\Gamma_2^x(k)\Gamma_2^y(-k)+\Gamma_3^x(k)\Gamma_3^y(-k)-\Gamma_4^x(k)\Gamma_4^y(-k)+c.c. \\
&+\Gamma_1^x(k)\Gamma_3^y(-k)-\Gamma_3^x(k)\Gamma_1^y(-k)-\Gamma_2^x(k)\Gamma_4^y(-k)+\Gamma_4^x(k)\Gamma_2^y(-k)-c.c.] \qquad (4.11)
\end{aligned}
$$

Again, the last four terms vanish in the integral over k.

Considering the exchange interactions, single ion anisotropy terms, and using the Fourier transform of the magnetic operators, we can develop the Hamiltonian on the whole lattice [52]:

$$
\begin{aligned}
H \;=\; &\frac{1}{4}\int_{\mathrm{BZ}} d^3k \sum_{ij}\Bigg[\mathcal{J}_1^{ij}\cos\frac{k_z}{2}(-\Gamma_1^i(k)\Gamma_1^j(-k)+\Gamma_2^i(k)\Gamma_2^j(-k)-\Gamma_3^i(k)\Gamma_3^j(-k)+\Gamma_4^i(k)\Gamma_4^j(-k)) \\
&+2\left(\mathcal{J}_2^{ij}\cos\frac{k_x}{2}\cos\frac{k_y}{2}+\mathcal{J}_3^{ij}\cos\frac{k_x}{2}\cos 3\frac{k_y}{2}\right) \\
&\qquad\times(-\Gamma_1^i(k)\Gamma_1^j(-k)+\Gamma_2^i(k)\Gamma_2^j(-k)+\Gamma_3^i(k)\Gamma_3^j(-k)-\Gamma_4^i(k)\Gamma_4^j(-k)) \\
&+D^{ij}(\Gamma_1^i(k)\Gamma_1^j(-k)+\Gamma_2^i(k)\Gamma_2^j(-k)+\Gamma_3^i(k)\Gamma_3^j(-k)+\Gamma_4^i(k)\Gamma_4^j(-k))\Bigg] \qquad (4.12)
\end{aligned}
$$

where $\mathcal{J}_n^{ij}=\mathcal{J}_n^{ji}$ $(n=1,2,3)$ are the six exchange couplings for each of the three paths and D^{ij}'s are the single ion anisotropy parameters. This is a general magnetic Hamiltonian which is suitable for a description of our magnetic system in terms of the magnetic operators. The Hamiltonian also represents the excitations in the system which will be discussed in Section 4.7. In general, the spin wave spectrum will become non-degenerate due to anisotropy in the exchange interactions and a mixing of polarizations in each mode is expected.

The most recent neutron scattering measurements by Senff *et al.* [53], show the mixing of magnon excitation modes in the spiral phase which are due to deviations from the

ideal cycloidal ordering. In fact, the real magnetic structure of $TbMnO_3$ is elliptical rather than circular [9] which leads to more complex interactions and mixing of polarizations. The magnetic Hamiltonian discussed above can describe the mixings in agreement with the experiment.

$\mathcal{J}_1^{ij}$, $\mathcal{J}_2^{ij}$ and $\mathcal{J}_3^{ij}$ are related to the exchange interaction parameters which were experimentally obtained by Takahashi *et al.* [49] as discussed in Section 3.4. The exchange constants are $J_1 = -0.85$ meV (ab plane), $J_2 = 0.68$ meV (ab plane) and $J_c = 1.28$ meV (c axis) and the single ion anisotropy $D = 0.13$ meV. J_1 is ferromagnetic (FM) while J_2 is antiferromagnetic (AFM). They confirmed that these values can produce the bc-spiral spin phase. Under the assumption that the parameters are isotropic, the experimentally obtained values J_1, J_2, J_c and D correspond to the theoretically derived parameters as follows: $J_1 = \mathcal{J}_2^{xx} = \mathcal{J}_2^{yy} = \mathcal{J}_2^{zz}$, $J_2 = \mathcal{J}_3^{xx} = \mathcal{J}_3^{yy} = \mathcal{J}_3^{zz}$, $J_c = \mathcal{J}_1^{xx} = \mathcal{J}_1^{yy} = \mathcal{J}_1^{zz}$ and $D = D^{xx} = D^{yy} = D^{zz}$.

4.6 Constraints on the System

Considering paths 1, 2 and 8, with 6 interaction terms on each path gives 18 exchange constants and 6 single ion anisotropy constants. The high-temperature phase (Phase I) is described by the order parameter $\Gamma_3^y(k)$ [9]. The Hamiltonian must be minimized at this wave vector k leading to the spiral arrangement of spins lying in the bc plane, which implies that $(-\mathcal{J}_1^{yy}/2 + \mathcal{J}_2^{yy}) \sin k_{\mathrm{Mn}}/2 + 3\mathcal{J}_3^{yy} \sin 3k_{\mathrm{Mn}}/2 = 0$. In addition, the sum of the coefficients of each of the terms $|\Gamma_1^i(k)|^2$, $|\Gamma_{2,4}^i(k)|^2$ and $|\Gamma_3^{x,z}(k)|^2$ must be positive. The coefficients of $\Gamma_1^x(k)\Gamma_1^y(-k)$ and similar terms are also constrained as follows.

For a Hamiltonian of the form:

$$\alpha(A^x)^2 + \beta A^x A^y + \gamma(A^y)^2$$

in order for all components of A to be stable, we must have $\alpha > 0$, $\gamma > 0$ and $\beta^2 < 4\alpha\gamma$. In order for only A^y to be unstable, need $\alpha > 0$, $\gamma < 0$ and $\beta = 0$. This means that the coefficients of $\Gamma_3^x(k)\Gamma_3^y(-k)$ and $\Gamma_3^z(k)\Gamma_3^y(-k)$ must vanish.

4.7 Spin Waves and Their Equations of Motion

In this part we look at the spin waves and their equations of motion. Spin wave theory makes use of an effective magnetic field [32]. For single spin sites, the effective field is:

$$B_{h,l}^m = -\frac{dH}{dJ_{h,l}^m}$$

where H is the Hamiltonian, J is the magnetic moment, $l = 1, 2, 3, 4$ is the sub-site index, $m = x, y, z$ and h is the site index. The equation of motion is then:

$$\frac{d\vec{J}_{h,l}}{dt} = -\vec{J}_{h,l} \times \vec{B}_{h,l}.$$

The Fourier transform of this is:

$$\begin{aligned}
\frac{d\vec{J}_l(\vec{k})}{dt} &= \sum_j e^{-i\vec{j}\cdot\vec{k}} \frac{d\vec{J}_l^{\vec{j}}}{dt} \\
&= \sum_j e^{-i\vec{j}\cdot\vec{k}} \vec{J}_l^{\vec{j}} \times \vec{B}_l^{\vec{j}} \\
&= \sum_j \left(\frac{abc}{(2\pi)^3}\right)^2 \int d^3k' d^3k'' e^{i\vec{j}\cdot(\vec{k}'+\vec{k}''-\vec{k})} \vec{J}_l(\vec{k}') \times \vec{B}_l(\vec{k}'') \\
&= \frac{abc}{(2\pi)^3} \int d^3k' \vec{J}_l(\vec{k}' + k) \times \vec{B}_l(-\vec{k}') \qquad (4.13)
\end{aligned}$$

where the Fourier transform of $\vec{B}$ is $B(-k) = \frac{dH}{dJ(k)}$. We can take this a step further and use the IR's at $Q = (0, k_{\mathrm{Mn}}, 0)$. The IR site operators are Γ_b^a, where $a = x, y, z$ and $b = 1, 2, 3, 4$. We have a set of transformations between Γ_l and J_l which are similar to Fourier transforms:

$$\Gamma_b^a(q) = \sum_{cd} \alpha_{bc}^a J_{d,c}^a e^{-iq(d+c)} \qquad (4.14)$$

where α_{bc} is obtained from Table 4.11,

$$\alpha^x = \begin{pmatrix} 1 & 1 & -1 & -1 \\ 1 & -1 & 1 & -1 \\ 1 & -1 & -1 & 1 \\ 1 & 1 & 1 & 1 \end{pmatrix}. \tag{4.15}$$

$$\alpha^y = \begin{pmatrix} 1 & -1 & -1 & 1 \\ 1 & 1 & 1 & 1 \\ 1 & 1 & -1 & -1 \\ 1 & -1 & 1 & -1 \end{pmatrix} \tag{4.16}$$

$$\alpha^z = \begin{pmatrix} 1 & -1 & 1 & -1 \\ 1 & 1 & -1 & -1 \\ 1 & 1 & 1 & 1 \\ 1 & -1 & -1 & 1 \end{pmatrix} \tag{4.17}$$

The equation of motion for the Γ's is:

$$\begin{aligned} \frac{d\Gamma_b^a(q)}{dt} &= \sum_{c=1}^{4}\sum_{d=1}^{N} \alpha_{bc}^a e^{-iq(d+c)} \frac{dJ_{d,c}^a}{dt} \\ &= \sum_{dcef} \epsilon^{aef} \alpha_{bc}^a e^{-iq(d+c)} J_{d,c}^e B_{d,c}^f \\ &= \sum_{dcefgq'} \frac{1}{4} \epsilon^{aef} e^{-iq(d+c)+iq'(d+c)} \alpha_{bc}^a \alpha_{gc}^e \Gamma_g^e(q') B_{d,c}^f. \end{aligned} \tag{4.18}$$

The most general form of the Hamiltonian is:

$$\begin{aligned} H &= \sum_{hijq''} C_h^{ij}(q'') \Gamma_h^i(q'') \Gamma_h^j(-q'') \\ &= \sum_{hijlmnoq''} C_h^{ij}(q'') \alpha_{hl}^i \alpha_{hm}^j J_{n,l}^i J_{o,m}^j e^{-iq''(n+l-o-m)} \end{aligned} \tag{4.19}$$

where $C_m^{ij}(q) = C_m^{ji}(q)$ are constant functions even in q. By comparing equations 4.12 and 4.19, we can find all the functions which are given below:

$$C_1^{ij}(q) = +\mathcal{J}_1^{ij}\cos\frac{k_z}{2} - \mathcal{J}_2^{ij}\cos\frac{k_x}{2}\cos\frac{k_y}{2} + \mathcal{J}_3^{ij}\cos\frac{k_x}{2}\cos 3\frac{k_y}{2} + D_{ij} \quad (4.20)$$

$$C_2^{ij}(q) = +\mathcal{J}_1^{ij}\cos\frac{k_z}{2} + \mathcal{J}_2^{ij}\cos\frac{k_x}{2}\cos\frac{k_y}{2} + \mathcal{J}_3^{ij}\cos\frac{k_x}{2}\cos 3\frac{k_y}{2} + D_{ij} \quad (4.21)$$

$$C_3^{ij}(q) = -\mathcal{J}_1^{ij}\cos\frac{k_z}{2} + \mathcal{J}_2^{ij}\cos\frac{k_x}{2}\cos\frac{k_y}{2} + \mathcal{J}_3^{ij}\cos\frac{k_x}{2}\cos 3\frac{k_y}{2} + D_{ij} \quad (4.22)$$

$$C_4^{ij}(q) = +\mathcal{J}_1^{ij}\cos\frac{k_z}{2} - \mathcal{J}_2^{ij}\cos\frac{k_x}{2}\cos\frac{k_y}{2} + \mathcal{J}_3^{ij}\cos\frac{k_x}{2}\cos 3\frac{k_y}{2} + D_{ij} \quad (4.23)$$

We find:

$$\begin{aligned} B_{d,c}^f &= \frac{dH}{dJ_{d,c}^f} \\ &= 2\sum_{hjmoq''} C_h^{fj}(q'')\alpha_{hc}^f\alpha_{hm}^j J_{o,m}^j e^{-iq''(d+c-o-m)} \\ &= 2\sum_{hjq''} C_h^{fj}(q'')\alpha_{hc}^f\Gamma_h^j(-q'')e^{-iq''(d+c)}, \end{aligned} \quad (4.24)$$

so finally:

$$\begin{aligned} \frac{d\Gamma_b^a(q)}{dt} &= \sum_{cdefghjq'q''} \epsilon^{aef}\alpha_{bc}^a\alpha_{gc}^e\alpha_{hc}^f C_h^{fj}(q'')\Gamma_g^e(q')\Gamma_h^j(-q'')e^{-i(q-q'+q'')(d+c)} \\ &= \sum_{cefghjq'} \epsilon^{aef}\alpha_{bc}^a\alpha_{gc}^e\alpha_{hc}^f C_h^{fj}(q'-q)\Gamma_g^e(q')\Gamma_h^j(q-q') \\ &= \sum_{cefghjq'} \epsilon^{aef}\alpha_{bc}^a\alpha_{gc}^e\alpha_{hc}^f C_h^{fj}(q')\Gamma_g^e(q'+q)\Gamma_h^j(-q'). \end{aligned} \quad (4.25)$$

The sums over e, f and c give the symmetry-expected terms which are in the form of $\Gamma_b = \Gamma_g \otimes \Gamma_h$ as shown in Table 4.13. For example, the only possible representation for $\Gamma_3 \otimes \Gamma_4$ is Γ_2.

We are interested in the high-temperature phase (phase I) which is described by $\Gamma_3^y(Q)$. We can simplify the equations by keeping terms only in the y directions and also considering

Γ_g \ Γ_h	Γ_1	Γ_2	Γ_3	Γ_4
Γ_1	Γ_1	Γ_2	Γ_3	Γ_4
Γ_2	Γ_2	Γ_1	Γ_4	Γ_3
Γ_3	Γ_3	Γ_4	Γ_1	Γ_2
Γ_4	Γ_4	Γ_3	Γ_2	Γ_1

Table 4.13: Product table for the representations of C_{2v}.

the particular Q vector. Keeping only Γ_3^ν, we find:

$$\begin{aligned}
\frac{d\Gamma_b^a(q)}{dt} &= \sum_{cfghjq'} \epsilon^{a\nu f}\alpha_{bc}^a\alpha_{gc}^\nu\alpha_{hc}^f C_h^{fj}(q')\Gamma_g^\nu(q'+q)\Gamma_h^j(-q') \\
&\quad + \sum_{cefghq'} \epsilon^{aef}\alpha_{bc}^a\alpha_{gc}^e\alpha_{hc}^f C_h^{f\nu}(q')\Gamma_g^e(q'+q)\Gamma_h^\nu(-q') \\
&= \sum_{cefghq'} \epsilon^{a\nu f}\alpha_{bc}^a\alpha_{gc}^\nu\alpha_{hc}^f C_h^{fe}(q')\Gamma_g^\nu(q'+q)\Gamma_h^e(-q') \\
&\quad + \sum_{cefghq'} \epsilon^{aef}\alpha_{bc}^a\alpha_{gc}^e\alpha_{hc}^f C_h^{f\nu}(q')\Gamma_g^e(q'+q)\Gamma_h^\nu(-q'). \qquad (4.26)
\end{aligned}$$

For the particular Q vector we consider $S = \Gamma_3^\nu(Q)$ and $S^* = \Gamma_3^\nu(-Q)$, we find:

$$\begin{aligned}
\frac{d\Gamma_b^a(q)}{dt} &= S\sum_{cefh} \epsilon^{a\nu f}\alpha_{bc}^a\alpha_{3c}^\nu\alpha_{hc}^f C_h^{fe}(q-Q)\Gamma_h^e(q-Q) \\
&\quad + S\sum_{cefg} \epsilon^{aef}\alpha_{bc}^a\alpha_{gc}^e\alpha_{3c}^f C_3^{f\nu}(Q)\Gamma_g^e(q-Q) \\
&\quad + S^*\sum_{cefh} \epsilon^{a\nu f}\alpha_{bc}^a\alpha_{3c}^\nu\alpha_{hc}^f C_h^{fe}(q+Q)\Gamma_h^e(q+Q) \\
&\quad + S^*\sum_{cefg} \epsilon^{aef}\alpha_{bc}^a\alpha_{gc}^e\alpha_{3c}^f C_3^{f\nu}(Q)\Gamma_g^e(q+Q)
\end{aligned}$$

$$
\begin{aligned}
&= S\sum_{cefh}\epsilon^{a\gamma f}\alpha^a_{bc}\alpha^\gamma_{3c}\alpha^f_{hc}C^{fe}_h(q-Q)\Gamma^e_h(q-Q)\\
&+S\sum_{cefh}\epsilon^{aef}\alpha^a_{bc}\alpha^e_{hc}\alpha^f_{3c}C^{f\gamma}_3(Q)\Gamma^e_h(q-Q)\\
&+S^*\sum_{cefh}\epsilon^{a\gamma f}\alpha^a_{bc}\alpha^\gamma_{3c}\alpha^f_{hc}C^{fe}_h(q+Q)\Gamma^e_h(q+Q)\\
&+S^*\sum_{cefh}\epsilon^{aef}\alpha^a_{bc}\alpha^e_{hc}\alpha^f_{3c}C^{f\gamma}_3(Q)\Gamma^e_h(q+Q). \qquad (4.27)
\end{aligned}
$$

Finally, the equations of motion for each representation are:

$$
\begin{aligned}
\frac{d\Gamma^a_1(q)}{dt} &= S\sum_{ef}\epsilon^{a\gamma f}C^{fe}_3(q-Q)\Gamma^e_3(q-Q)+S\sum_{ef}\epsilon^{aef}C^{f\gamma}_3(Q)\Gamma^e_3(q-Q)\\
&+S^*\sum_{ef}\epsilon^{a\gamma f}C^{fe}_3(q+Q)\Gamma^e_3(q+Q)+S^*\sum_{ef}\epsilon^{aef}C^{f\gamma}_3(Q)\Gamma^e_3(q+Q) \qquad (4.28)\\
\frac{d\Gamma^a_2(q)}{dt} &= S\sum_{ef}\epsilon^{a\gamma f}C^{fe}_4(q-Q)\Gamma^e_4(q-Q)+S\sum_{ef}\epsilon^{aef}C^{f\gamma}_3(Q)\Gamma^e_4(q-Q)\\
&+S^*\sum_{ef}\epsilon^{a\gamma f}C^{fe}_4(q+Q)\Gamma^e_4(q+Q)+S^*\sum_{ef}\epsilon^{aef}C^{f\gamma}_3(Q)\Gamma^e_4(q+Q) \qquad (4.29)\\
\frac{d\Gamma^a_3(q)}{dt} &= S\sum_{ef}\epsilon^{a\gamma f}C^{fe}_1(q-Q)\Gamma^e_1(q-Q)+S\sum_{ef}\epsilon^{aef}C^{f\gamma}_3(Q)\Gamma^e_1(q-Q)\\
&+S^*\sum_{ef}\epsilon^{a\gamma f}C^{fe}_1(q+Q)\Gamma^e_1(q+Q)+S^*\sum_{ef}\epsilon^{aef}C^{f\gamma}_3(Q)\Gamma^e_1(q+Q) \qquad (4.30)\\
\frac{d\Gamma^a_4(q)}{dt} &= S\sum_{ef}\epsilon^{a\gamma f}C^{fe}_2(q-Q)\Gamma^e_2(q-Q)+S\sum_{ef}\epsilon^{aef}C^{f\gamma}_3(Q)\Gamma^e_2(q-Q)\\
&+S^*\sum_{ef}\epsilon^{a\gamma f}C^{fe}_2(q+Q)\Gamma^e_2(q+Q)+S^*\sum_{ef}\epsilon^{aef}C^{f\gamma}_3(Q)\Gamma^e_2(q+Q) \qquad (4.31)
\end{aligned}
$$

The above complicated set of equations can be simplified by keeping only symmetric terms

in H as follows:

$$\begin{aligned}
\frac{d\Gamma_1^a(q)}{dt} &= S\sum_e \epsilon^{aye} C_3^{ee}(q-Q)\Gamma_3^e(q-Q) + S\sum_e \epsilon^{aey} C_3^{yy}(Q)\Gamma_3^e(q-Q) \\
&\quad + S^*\sum_e \epsilon^{aye} C_3^{ee}(q+Q)\Gamma_3^e(q+Q) + S^*\sum_e \epsilon^{aey} C_3^{yy}(Q)\Gamma_3^e(q+Q) \\
\frac{d\Gamma_1^x(q)}{dt} &= S(C_3^{zz}(q-Q) - C_3^{yy}(Q))\Gamma_3^z(q-Q) + S^*(C_3^{zz}(q+Q) - C_3^{yy}(Q))\Gamma_3^z(q+Q) \\
\frac{d\Gamma_1^z(q)}{dt} &= S(C_3^{yy}(Q) - C_3^{xx}(q-Q))\Gamma_3^x(q-Q) - S^*(C_3^{xx}(q+Q) - C_3^{yy}(Q))\Gamma_3^x(q+Q)
\end{aligned} \tag{4.32}$$

$$\begin{aligned}
\frac{d\Gamma_2^a(q)}{dt} &= S\sum_e \epsilon^{aye} C_4^{ee}(q-Q)\Gamma_4^e(q-Q) + S\sum_e \epsilon^{aey} C_3^{yy}(Q)\Gamma_4^e(q-Q) \\
&\quad + S^*\sum_e \epsilon^{aye} C_4^{ee}(q+Q)\Gamma_4^e(q+Q) + S^*\sum_e \epsilon^{aey} C_3^{yy}(Q)\Gamma_4^e(q+Q) \\
\frac{d\Gamma_2^x(q)}{dt} &= S(C_4^{zz}(q-Q) - C_3^{yy}(Q))\Gamma_4^z(q-Q) + S^*(C_4^{zz}(q+Q) - C_3^{yy}(Q))\Gamma_4^z(q+Q) \\
\frac{d\Gamma_2^z(q)}{dt} &= S(C_3^{yy}(Q) - C_3^{xx}(q-Q))\Gamma_4^x(q-Q) - S^*(C_4^{xx}(q+Q) - C_3^{yy}(Q))\Gamma_4^x(q+Q)
\end{aligned} \tag{4.33}$$

$$\begin{aligned}
\frac{d\Gamma_3^a(q)}{dt} &= S\sum_e \epsilon^{aey} C_1^{ee}(q-Q)\Gamma_1^e(q-Q) + S\sum_e \epsilon^{aey} C_3^{yy}(Q)\Gamma_1^e(q-Q) \\
&\quad + S^*\sum_e \epsilon^{aye} C_1^{ee}(q+Q)\Gamma_1^e(q+Q) + S^*\sum_e \epsilon^{aey} C_3^{yy}(Q)\Gamma_1^e(q+Q) \\
\frac{d\Gamma_3^x(q)}{dt} &= S(C_1^{zz}(q-Q) - C_3^{yy}(Q))\Gamma_1^z(q-Q) + S^*(C_1^{zz}(q+Q) - C_3^{yy}(Q))\Gamma_1^z(q+Q) \\
\frac{d\Gamma_3^z(q)}{dt} &= S(C_3^{yy}(Q) - C_1^{xx}(q-Q))\Gamma_1^x(q-Q) - S^*(C_1^{xx}(q+Q) - C_3^{yy}(Q))\Gamma_1^x(q+Q)
\end{aligned} \tag{4.34}$$

$$
\begin{aligned}
\frac{d\Gamma_4^a(q)}{dt} &= S\sum_e \epsilon^{aye} C_2^{ee}(q-Q)\Gamma_2^e(q-Q) + S\sum_e \epsilon^{aey} C_3^{yy}(Q)\Gamma_2^e(q-Q) \\
&\quad + S^*\sum_e \epsilon^{aye} C_2^{ee}(q+Q)\Gamma_2^e(q+Q) + S^*\sum_e \epsilon^{aey} C_3^{yy}(Q)\Gamma_2^e(q+Q) \\
\frac{d\Gamma_4^x(q)}{dt} &= S(C_2^{zz}(q-Q) - C_3^{yy}(Q))\Gamma_2^z(q-Q) + S^*(C_2^{zz}(q+Q) - C_3^{yy}(Q))\Gamma_2^z(q+Q) \\
\frac{d\Gamma_4^z(q)}{dt} &= S(C_3^{yy}(Q) - C_2^{xx}(q-Q))\Gamma_2^x(q-Q) - S^*(C_2^{xx}(q+Q) - C_3^{yy}(Q))\Gamma_2^x(q+Q)
\end{aligned}
\tag{4.35}
$$

The symmetric case leads to a more simplified set of equations. As it was discussed in Section 4.5 a mixing of spin-wave polarizations is expected in the magnetic Hamiltonian (Eq. 4.12), because of including the antisymmetric terms in the exchange interactions. However, in the symmetric case relations such as $\frac{d^2\Gamma_1^x(q)}{dt} \sim \frac{d\Gamma_3^z(q)}{dt} \sim \Gamma_1^x$ show that IR's are decoupled and all mixings vanish due to degeneracy in the spin-wave spectrum.

In this chapter we limit our discussion to a simplified magnetic Hamiltonian by considering only the magnetic operators for Mn ions and ignoring the interactions due to Tb sublattice. The Hamiltonian describes the mixings in agreement with the experiments [9, 53]. We also derived a simplified set of equations of motion for spin waves by keeping only $\Gamma_3^y(Q)$ and the symmetric terms. Although we limit this discussion to simple mathematical models, our group theoretical approach is capable of describing the phenomenology of $TbMnO_3$ in the most general way and can be applied to study other spiral multiferroics.

Chapter 5

Conclusions and Outlook

5.1 Conclusions

The overall objective of this research was to study the phenomenology of the spiral magnet $TbMnO_3$ by looking at symmetry properties of the magnetic space group. This work can be divided into three major sections:

(1) The first part was an extensive study of the magnetic phase transitions due to Mn sublattice by considering the symmetry breaking associated with each phase transition. Our symmetry analysis revealed the allowed symmetry elements in the spiral phase of spins. It was also shown that Mn magnetic operators are even under inversion while Tb moments correspond to both even and odd magnetic operators.

(2) The most general form of the magnetic Hamiltonian was developed based on the nearest and next nearest neighbor interactions and single ion anisotropy terms. The analyses were extended to include both symmetric and anti-symmetric interactions. Minimizing the Hamiltonian at the wave vector $(0, k, 0)$, showed the constraints on the coefficients, the coupling constants and the corresponding IR for the spins configuration. The Hamiltonian also describes excitations in the system, namely spin waves. Generally speaking, the spin

wave spectrum will become non-degenerate due to anisotropy in the exchange interaction, and a mixing of polarizations in each mode can be expected. The mixings correspond to the deviations from the ideal cycloidal ordering of the spins in agreement with recent neutron scattering measurements [9, 53].

(3) Detailed study of spin waves led us to derive the equations of motions in terms of the magnetic operators. The equations were particularly studied in the high-temperature phase (phase I) by keeping terms in the form of $\Gamma_3^y(Q)$ which are magnetic operators in the y direction and at a particular wave vector Q. The equations of spin waves form a coupled set which is complicated to solve. Therefore, we simplified the problem by only looking at the symmetric terms. In this case the polarizations are decoupled and polarized spin waves are expected.

5.2 Outlook

In this thesis we assumed that there is no coupling between Mn and Tb sublattices. To derive a more realistic magnetic Hamiltonian, it is essential to consider the interactions due to terbium ions and the coupling between the two sublattices. A set of Tb magnetic operators can be derived in the same way as for the Mn ions and these operators can be included in a more complete Hamiltonian.

A detailed study of the magnetic phase transitions of terbium sublattice, its interactions with manganese ions and the corresponding magnetic operators are suggested.

Solving the set of equations of motion for spin waves leads us to derive the dispersion relations for our magnetic system. The coupled set of equations is complicated to be solved analytically. In this thesis we considered the symmetric case which simplifies the equations into decoupled IR's. Perturbation methods are suggested to find approximate but more realistic solutions.

We used the experimental results of Ref. [9] to study the phase transitions, symmetry breaking and spin configurations in different phases. We also discussed the connections between our magnetic Hamiltonian with the experimental results on the exchange couplings from Ref. [49] and the mixing of polarizations from Ref. [9, 53]. Further studies and deriving more realistic models as discussed above can reveal more sophisticated connections between our theoretical results and the experiments.

We particularly focused on phase I with the sinusoidal antiferromagnetic arrangement of spins. As discussed in Section 3.3, the magnetic order in phase I is described by only one IR, Γ_3^y. In the low-temperature phase (phase II), an x component of Γ_2 also appears which together with the y component of Γ_3 best describe the spiral phase. By including Γ_2^x in the equations of motion, we can describe the more complex state in the low-temperature phase.

Finally, this theoretical study can be extended to include the terms which couple spin and electric polarization. In general, we can introduce a magnetoelectric coupling term in a Landau expansion which is invariant under all symmetry elements of the space group. From the microscopic point of view, the spin Hamiltonian must contain the coupling of two magnetic order parameters and one displacement operator with the corresponding irreps which characterize the magnetic and ferroelectric orderings.

Bibliography

[1] P. Curie, *J. Phys. Theor. Appl.* **3**, 393-415 (1894).

[2] L. D. Landau and E. M. Lifshitz, *Electrodynamics of continuous media* (Fizmatgiz Moscow 1959).

[3] I. E. Dzyaloshinskii, *Sov. Phys. JETP* **10**, 628 (1959).

[4] D. N. Astrov, *Sov. Phys. JETP* **11**, 708 (1609).

[5] H. Schmid, *Ferroelectrics* **162**, 317 (1994).

[6] D. Khomskii, *APS Trends Physics* **2**, 20 (2009).

[7] C. Michel, J. M. Moreau, G. D. Achenbach, R. G. and W. J. James, *Solid State Commun.* **7**, 701704 (1969).

[8] T. Kimura, T. Goto, H. Shintani, K. Ishizaka, T. Arima and Y. Tokura1, *Nature* **426**, 55-58 (2003).

[9] M. Kenzelmann, A. B. Harris, S. Jonas, C. Broholm, J. Schefer, S. B. Kim, C. L. Zhang, S. W. Cheong, O. P. Vajk, and J.W. Lynn, *Phys. Rev. Lett.*, **95**, 087206 (2005).

[10] T. Kimura, *Annu. Rev. Mater. Res.* **37**, 387413 (2007).

[11] H. Katsura, N. Nagaosa and A. V. Balatsky, *Phys. Rev. Lett.* **95**, 057205 (2005).

[12] M. Mostovoy, *Phys. Rev. Lett.* **96**, 067601 (2006).

[13] T. Arima, Y. Yamasaki, T. Goto, S. Iguchi, K. Ohgushi, S. Miyasaka, and Y. Tokura, *J. Phys. Soc. Jpn* **76**, 023602 (2007).

[14] P. W. Anderson, *Phys. Rev.* **115**, 1 (1959).

[15] T. Moriya, *Phys. Rev.* **120**, 1 (1960).

[16] T. Moriya, *Phys. Rev. Lett.* **4**, 228 (1960).

[17] T. Moriya, *Phys. Rev. Lett.* **4**, 5 (1960).

[18] I. A. Sergienko and E. Dagotto, *Phys. Rev. B* **73**, 094434 (2006).

[19] A. B. Harris, *Phys. Rev. B* **76**, 054447 (2007).

[20] P. G. Radaelli and L. C. Chapon, *Phys. Rev. B* **76**, 054428 (2007).

[21] T. Kimura and Y. Tokura *J. Phys. Condens. Matter* **20**, 434204 (2008).

[22] T. Kimura, Y. Sekio, H. Nakamura, T. Siegrist and A. P. Ramirez, *Nature Materials*, **7**, 291-294 (2008).

[23] T. Kimura, G. Lawes, T. Goto, Y. Tokura, A. P. Ramirez, *Phys. Rev. B* **71**, 224425 (2005).

[24] W. Eerenstein, N. D. Mathur and J. F. Scott, *Nature*, **442**, 759-765 (2008).

[25] N. Hur, S. Park, P. A. Sharma, J. S. Ahn, S. Guha, and S.-W. Cheong, *Nature*, **429**, 392 (2004).

[26] S.-W. Cheong and M. Mostvoy, *Nature Mater*, **6**, 13 (2007).

[27] M. Fiebig, *J. Phys. D*, **38**, R123 (2005).

[28] D. N. Argyriou, N. Aliouane, J. Strempfer, I. Zegkinoglou, B. Bohnenbuck, K. Habicht and M. v. Zimmermann, *Phys. Rev. B*, **75**, 020101(R) (2007).

[29] D. Senff, P. Link, N. Aliouane, D. N. Argyriou and M. Braden, *Phys. Rev. B*, **77**, 174419 (2008).

[30] M. Tinkham, *Group Theory and Quantum Mechanics* (McGraw-Hill US 1964).

[31] K. F. Reley, M. P. Hobson, S. J. Bence, *Mathematical Methods for Physics and Engineering* (Cambridge University Press UK 2006).

[32] Charles Kittel, *Introduction to Solid State Physics* (John Wiley & Sons 2005)

[33] Hans-Waldemar Streitwolf, *Group Theory in Solid-State Physics* (Macdonald London 1971).

[34] C. J. Bradley, A. P. Cracknell, *The Mathematical Theory of Symmetry in Solids* (Clarendon Oxford 1972).

[35] Edited by: Theo Hahn, *International Tables for Crystallography* (D. Reidel USA 1983).

[36] J. C. Tolédano, P. Tolédano, *The Landau Theory of Phase Transitions* (World Scientific 1987).

[37] S. Quezel, F. Tcheou, J. Rossat-Mignod, G. Quezel and E. Roudaut, *Physica B* **86-88B**, 916 (1977).

[38] J. A. Alonso, M. J. Martínez-Lope, M. T. Casais and M. T. Fernández-Díez, *Inorg. Chem.* **39**, 917 (2000).

[39] D. Meier, N. Aliouane, D. N. Argyriou, J. A. Mydosh and T. Lorenz, *NJP* **9**, 100 (2007).

[40] J. Blasco, C. Ritter, J. Garca, J. M. de Teresa, J. Prez-Cacho, and M. R. Ibarra, *Phys. Rev. B* **62**, 5609 (2000).

[41] R. Kajimito, H. Yoshizawa, H. Shintani, T. Kimura and Y. Tokura, *Phys. Rev. B* **70**, 012401 (2004).

[42] A. B. Harris, G. Lawes, *Handbook of Magnetism and Advanced Magnetic Materials* (John Wiley Sons 2007).

[43] P. Tolédano, *Phys. Rev. B* **79**, 094416 (2009).

[44] V. Scagnoli, S. W. Lovesey, *Phys. Rev. B* **79**, 035111 (2009).

[45] D. Mannix, D. F. McMorrow, R. A. Ewings, A. T. Boothroyd, D. Prabhakaran, Y. Joly, B. Janousova, C. Mazzoli, L. Paolasini and S. B. Wilkins, *Phys. Rev. B* **76**, 184420 (2007).

[46] J. Voigt, J. Persson, J. W. Kim, G. Bihlmayer and Th. Brckel, *Phys. Rev. B* **76**, 104431 (2007)

[47] T. Kimura, S. Ishihara, H. Shintani, T. Arima, K. T. Takahashi, K. Ishizaka and Y. Tokura, *Phys. Rev. B* **68**, 060403 (2003).

[48] A. Pimenov, A. Shuvaev, A. Loidl, F. Schrettle, A. A. Mukhin, V. D. Travkin, V. Yu. Ivanov and A. M. Balbashov, *Phys. Rev. Lett.* **102**, 107203 (2009).

[49] Y. Takahashi, N. Kida, Y. Yamasaki, J. Fujioka, T. Arima, R. Shimano, S. Miyahara, M. Mochizuki, N. Furukawa and Y. Tokura, *Phys. Rev. Lett.* **101**, 187201 (2008).

[50] D. Seeff, P. Link, K. Hradil, A. Hiess, L. P. Regnault, Y. Sidis, N. Aliouane, D. N. Argyriou and M. Braden, *Phys. Rev. Lett.* **98**, 137206 (2007).

[51] A. Yoshimori, *J. Phys. Soc. Jpn.* **14**, 807 (1959).

[52] Arash A. Samimi, S. H. Curnoe, *Journal of Physics: Conference Series* (submitted) (ICM 2009)

[53] D. Senff, N. Aliouane, D. N. Argyriou, A. Hiess, L. P. Regnault, P. Link, K. Hradil, Y. Sidis, M. Braden, *J. Phys.: Condens. Matter* **20**, 434212 (2007).